

Organic matter distribution and retention along transects from hilltop to kettle hole within an agricultural landscape

Kai Nils Nitzsche · Michael Kaiser · Katrin Premke · Arthur Gessler ·
Ruth Heike Ellerbrock · Carsten Hoffmann · Andreas Kleeberg ·
Zachary Eric Kayler

Received: 8 February 2017 / Accepted: 14 September 2017 / Published online: 26 September 2017
© Springer International Publishing AG 2017

Abstract In agricultural landscapes, the spatio-temporal distribution of organic matter (OM) varies greatly across landscape structures and soil types. We investigated patterns of organic carbon (OC) content, polyvalent cations, and isotopic values for specific OM fractions along transects spanning topographic positions from erosional to depositional areas, including aquatic sediments within a single kettle hole. We hypothesized different drivers exist at different scales. At the transect scale, we hypothesized (1) landscape form and land management to explain patterns of isotopic and OC content from different OM

fractions. At the aggregate scale, (2) we expected different OM-mineral associations to explain stabilized OM. We also hypothesized, (3) that shallow sediment $\delta^{13}\text{C}$ and $\delta^{15}\text{N}$ of the kettle hole reflected different terrestrial sources. We found that distinct differences in the OM turnover rates existed between the fractions suggesting that different processes are affecting the transformation rates that are recorded in the isotopic composition patterns. Erosion along with plant productivity drive mineral-associated fractions over the transect, while microbial decomposition and slurry influence freely available and aggregated OM fractions. The type and magnitude of OM-mineral

Responsible Editor: Jan mulder.

K. N. Nitzsche (✉) · K. Premke · A. Gessler ·
Z. E. Kayler (✉)
Leibniz Centre for Agricultural Landscape Research
(ZALF), Institute of Landscape Biogeochemistry,
Eberswalder Str. 84, 15374 Muencheberg, Germany
e-mail: kai.nitzsche@chikyu.ac.jp

Z. E. Kayler
e-mail: zkayler@uidaho.edu

M. Kaiser
Department of Environmental Chemistry, University of
Kassel, Nordbahnhofstr. 1a, 37213 Witzenhausen,
Germany

K. Premke
Leibniz-Institute of Freshwater Ecology and Inland
Fisheries, Chemical Analytic and Biogeochemistry,
Mueggelseedamm 310, 12587 Berlin, Germany

A. Gessler
Swiss Federal Institute for Forest, Snow and Landscape
Research (WSL), Zuercherstrasse 111, 8903 Birmensdorf,
Switzerland

A. Gessler
Berlin-Brandenburg Institute of Advanced Biodiversity
Research (BBIB), 14195 Berlin, Germany

R. H. Ellerbrock · C. Hoffmann
Leibniz Centre for Agricultural Landscape Research
(ZALF), Institute of Soil Landscape Research,
Eberswalder Str. 84, 15374 Muencheberg, Germany

C. Hoffmann
Leibniz Centre for Agricultural Landscape Research
(ZALF), Agricultural Landscape Data Centre,
Eberswalder Str. 84, 15374 Muencheberg, Germany

associations changed along the transect while binding OM of different decomposition status. OM in mineral-associated fractions in kettle hole sediments were derived from clay- and silt-sized particles from the field, whereas OM in freely available and aggregated fractions potentially originated from macrophytes. We conclude that kettle holes constitute important sinks for terrestrial OM across the landscape.

Keywords Stable isotopes · Erosion · Soil organic matter · Organo-mineral interaction · Land management · Depressional wetland

Introduction

Agricultural landscapes encompass multiple land-use histories, landscape structures, soil types, and water paths leading to a region characterized by high levels of environmental and biogeochemical heterogeneity (Nitzsche et al. 2016). This is especially apparent where aquatic and terrestrial domains converge creating transition zones in environmental variables, such as soil moisture, redox potential, and microclimate (Stallard 1998; Cole et al. 2007; Premke et al. 2016). The distribution of organic matter (OM) also varies in catchments as erosion transfers material from the terrestrial to the aquatic domain (Doetterl et al. 2016; Hu et al. 2016; Nitzsche et al. 2017) or plant derived OM contributions increase in soil with greater soil moisture content near the water body. Erosion, accelerated by tillage, might also alter the distribution

of soil particles of various sizes as well as polyvalent cations involved in organo-mineral associations. Fertilization can also affect spatial patterns of productivity and corresponding OM inputs into the soil (Berhe et al. 2012; Kirkels et al. 2014). Consequently, patterns in soil OM emerge from the relative influence of environmental gradients, sources of OM, and management practices across different spatial scales.

Landscape topography plays an important role in OM distribution (Doetterl et al. 2016), and terrain attributes, inferred from digital elevation models, for example, have been widely used to predict soil organic matter (SOM) distribution. For instance, concave slopes, indicated by negative curvature, are considered areas of SOM accumulation, while convex slopes are represented by positive curvature, which are prone to erosion (Liu et al. 2013). Other indices (e.g., topographic position index (TPI) and topographic wetness index (TWI)) can convey information about the large-scale landscape characteristics as they relate to the variability in OM distribution, erosion, and plant productivity. These indicators may help in characterizing OM exposure to microbial processing, incorporation of plant assimilates, or the degree to which OM has been transported down a hillslope. Models that incorporate these spatial and temporal processes reveal not only the impact of any single parameter, such as soil texture, but also capture landscape level turnover time of OM.

Soil erosion leads to the downslope transport of OM and soil particles from hilltops to areas of deposition, exposing lower soil horizons in some cases at erosional positions, thus creating gradients in nutrients, soil moisture, and soil chemistry (Doetterl et al. 2016). Accordingly, eroded soils may exhibit reduced nutrient content and water holding capacity due to leaching, the destruction of the physical soil matrix, and the accompanied washout of nutrient-adsorbing clays, potentially reducing soil fertility and plant productivity on eroding slopes. Simultaneously, soil fertility may increase in depositional areas due to the additional SOM. Especially clay sized mineral particles and aggregates > 53 μm are usually enriched in organic carbon (OC) relative to the bulk soil. These particles and micro-aggregates are generally comprised of complexed, poorly crystalline and well-crystallized mineral phases as well as clay minerals (e.g., oxides, layer-silicates) that can interact with OM (Kaiser et al. 2007; Doetterl et al. 2015). Thus, OM

A. Kleeberg
State Laboratory Berlin-Brandenburg, Department
Geology, Soil, Waste, Stahnsdorfer Damm 77,
14532 Kleinmachnow, Germany

Z. E. Kayler
Lawrence Livermore National Laboratory, Center for
Accelerator Mass Spectrometry, Livermore, CA 94550,
USA

Z. E. Kayler
Department of Soil and Water Systems, University of
Idaho, Moscow, ID 83843, USA

Present Address:
K. N. Nitzsche
Research Institute for Humanity and Nature (RIHN), 457-4
Motoyama, Kamigamo, Kita-ku, Kyoto 603-8047, Japan

bound in micro-aggregates $< 53 \mu\text{m}$ and attached to mineral surfaces can be transported into small water bodies via erosion (Stallard 1998) and contribute to the C storage potential of the landscape (Premke et al. 2016). While, erosion distributes poorly crystalline mineral phases over the landscape (Berhe et al. 2012; Ellerbrock et al. 2016), the source of OM (e.g., poorly vs. strongly microbially processed) associated with these mineral phases remains largely unknown.

An understanding of the key factors and processes that regulate OM stabilization in soils requires the separation of OM fractions stabilized according to specific mechanisms (Mikutta et al. 2006). OM stabilization in aerated mineral soils results from (i) interactions of the OM with polyvalent cations (chelate, crosslinking) (e.g., Masiello et al. 2004; Mouvenchery et al. 2012), (ii) associations of the OM with mineral surfaces via polyvalent cations (cation bridges) (von Lützow et al. 2006), or (iii) direct bond formation between OM and mainly Fe- or Al-oxides (ligand exchange reactions) (Mikutta et al. 2007; Kleber et al. 2015). Stabilization mechanisms of OM in aquatic sediments may substantially differ from soils given that they are permanently water saturated (Hedges and Oades 1997). Currently, adsorption of

OM to mineral surfaces is considered the major stabilization mechanism in sediments (Mayer 1994; Hedges and Keil 1995). Recently, Lalonde et al. (2012) found a preferential stabilization of OM via reactive iron surfaces in sediments globally; however, it is not known whether or not these findings hold for smaller water bodies in an agricultural setting, such as kettle holes—small ($< 1 \text{ ha}$) depressional wetlands characterized by fluctuating waters levels (Kalettka and Rudat 2006).

Across a toposequence in a kettle hole catchment of the moraine landscape of NE Germany, where erosion is ubiquitous, we investigated patterns of OM stabilization and assessed OM sources along transects spanning topographic positions from erosional hilltops and hillslopes to depositional footslopes and edges, extending to sediments within a single kettle hole (Fig. 1). This toposequence spans a gradient in environmental conditions, for example, soil moisture and redox potential. We used OM fractions (i.e., organic particles, water extractable OM, and mineral associated OM) from these topographic positions separated by sequential fractionation (Kaiser et al. 2010, 2012). The susceptibility of OM in these fractions to erosion or mineralization with respect to

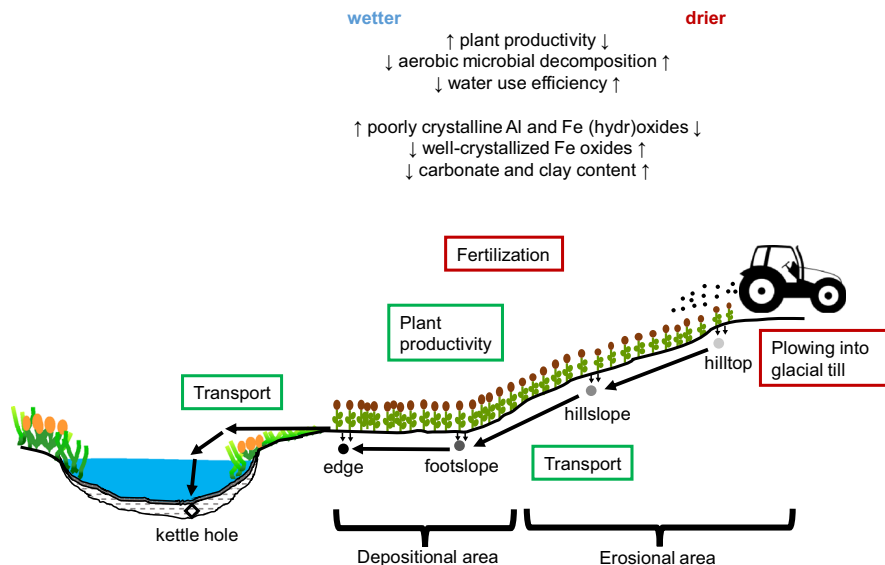


Fig. 1 Schematic cross-section through the catchment of the kettle hole. Differences in biological activity and soil mineral and environmental characteristics between depositional (wetter) and erosional (drier) areas are highlighted with upward arrows (increase) and downward arrows (decrease). Black arrows

highlight primary organic matter inputs (transport and plant productivity in green boxes) that contribute to the OM $\delta^{13}\text{C}$ and $\delta^{15}\text{N}$ at each topographic position. Land-management activities are indicated by red boxes. Sampling positions are shown by filled circles (soil) and the open diamond (sediment)

prevailing environmental conditions differs; therefore, we used the stable isotope composition of OM fractions to infer OM fate and origin (Sollins et al. 2009; Kayler et al. 2011; Schrumpp and Kaiser 2015).

We related OM isotopic data to landscape proxies (TPI, TWI) and leaf area index (LAI) to estimate the effects of landscape topography and plant productivity on OM dynamics. We hypothesized: (1) at the transect scale, topography would explain the variability in the OC contents and the $\delta^{13}\text{C}$ and $\delta^{15}\text{N}$ of bulk soil, sediment, and OM fractions. We also used an isotopic distillation model that accounts for the changes in isotopic composition of OM and the corresponding OC concentration to infer the impact of mass transport, OM source contributions, and possible impacts of management. (2) At the aggregate scale (i.e., soil fractions), we expected OM to be stabilized via different binding mechanisms that reflect potentially strong gradient in cations, crystalline and non-crystalline oxides, and clay- and silt-sized soil particles induced by erosion. Given the close proximity of the kettle hole and hillslope we hypothesized, (3) surface sediment $\delta^{13}\text{C}$ and $\delta^{15}\text{N}$ will reflect input from different terrestrial sources.

Materials and methods

Study site

The study site is located in the Quillow catchment ($\sim 168 \text{ km}^2$) as part of the young and hummocky moraine plain of NE Germany, formed after the end of the Weichsel glaciation approximately 12,000 to 10,000 years ago, that is intensively used for agriculture. Within the landscape, around 150,000 to 300,000 kettle holes exist (Kalettka and Rudat 2006). We selected a single kettle hole surrounded by an agricultural field (E013°39'57", N53°23'51") and located in the center of a runoff catchment area (3.4 ha) near the village Kraatz. Elevation ranged from 88.2 m to 101.1 m a.s.l and slopes were short and steep and as high as 7.9° (Fig. 2). This kettle hole has been under intense investigation since autumn 2012 within the project LandScales 'Connecting processes and structures driving landscape carbon dynamics over scales'. The climate is sub humid with an average annual temperature of 8.6°C and average annual precipitation of 499 mm between 1992 and

2013 (AgroScapeLab Quillow, Dedelow, E013°48'12", N53°21'59").

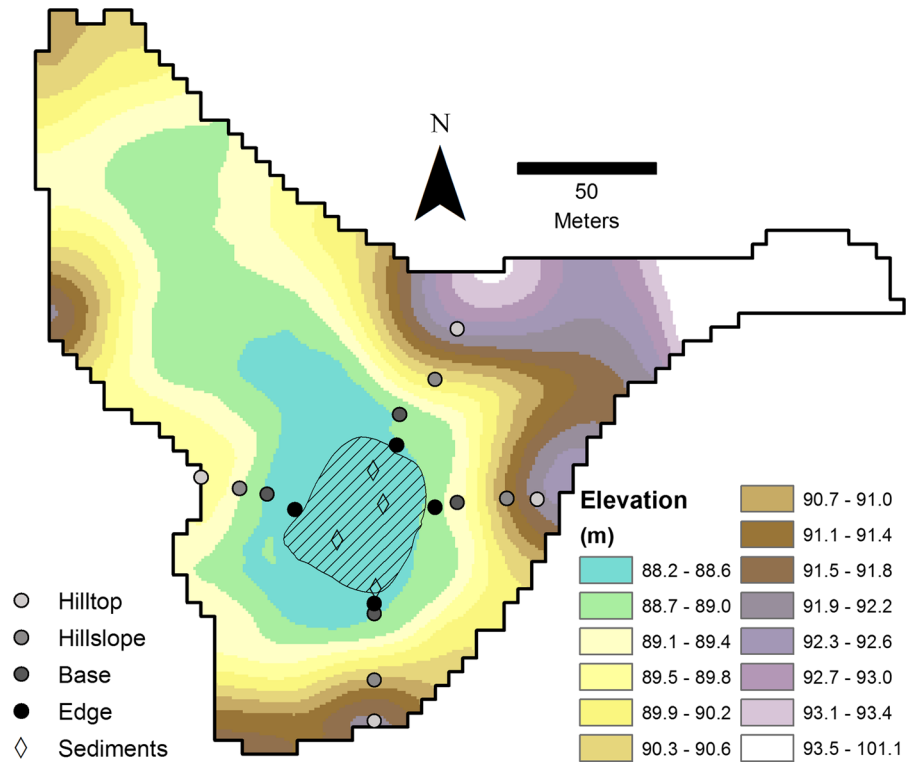
In hummocky, agricultural landscapes, characteristic soil types at hilltops and upper slope positions are Calcaric Regosols and Calcic Luvisols, which are strongly eroded into the subsoil. In depressions, nearby the kettle hole, Colluvic Regosols with a M-horizon thicker than 50 cm dominate, which developed under groundwater and stagnant water (Gleysols, Stagnosols). For two hilltop and two hillslope locations, the C-horizon was near the surface (23–37 cm) and already strongly mixed into the Ap horizon. In the depositional area around the kettle hole, the C-horizon was more than 150 cm below the surface.

The field has been under agricultural use for several centuries, and since the 1950s the field has been cultivated with a rotation of winter wheat (*Triticum aestivum*)—winter barley (*Hordeum vulgare*)—rape-seed (*Brassica napus*). Rape-seed was cultivated in 2013. Annual plowing was common until 2005 at a depth of approximately 35 cm, thereafter plowing occurred every third year. Slurry from a nearby pig farm has been applied approximately since 1980 amounting to $135 \text{ kg N ha}^{-1} \text{ a}^{-1}$. The last slurry application prior to sampling was in August 2012. Additional chemical fertilizers have been applied since the second half of the nineteenth century to fulfill the crop-specific N demand (for winter wheat $220 \text{ kg N ha}^{-1} \text{ a}^{-1}$, for winter barley $170 \text{ kg N ha}^{-1} \text{ a}^{-1}$, and for rape-seed $200 \text{ kg N ha}^{-1} \text{ a}^{-1}$).

Sampling design

In 2013, we collected topsoil samples (0–15 cm) from the kettle hole catchment. Many flow paths of OM including run-off occur within kettle hole catchments. These flow paths could lead to high variability in biotic and abiotic influences on the OM distribution across the catchments. We therefore focused our sampling efforts on a single kettle hole to better understand mechanisms behind OM stabilization rather than on OM variability across several kettle holes. We sampled four transects consisting of four slope positions (hilltop, hillslope, footslope, depression edge) terminating with one position in the kettle hole (Figs. 1, 2) leading to four samples per slope position and amounting to a total of 20 plots ($n = 20$); thus, we

Fig. 2 Elevation (m) of the catchment with sampling locations (filled circles for soils and open diamonds for sediments)



have sixteen individual plots along the hillside resulting in four plots at each terrestrial position and four plots within the kettle hole. At each slope position, we took three subsamples of 100 g soil each in a 1 m² area and mixed the samples afterward. We sampled sediment cores from the kettle hole with a sediment corer (UWITEC, Austria, i.d., 60 mm). The water level during the time of sampling was approximately 1 m. Sampling positions in the kettle holes were considered an extension of the four transects. Sediment sample depth encompassed 2–7 cm, we removed the top two cm due to this layer containing primarily fresh, recently, deposited OM. All samples were stored in gas-tight containers at 4 °C in dark conditions prior to preparation. Soil and sediment samples were air-dried and passed through a 2 mm sieve.

Leaf area index and bulk density

We quantified leaf area index (LAI) using a SunScan (Delta-T Devices Ltd.) device biweekly during April

and July 2014 for wheat and 2015 for barley along eight sampling points near our southern and eastern transects (max. \pm 2 m). From these measurements we used the maximum LAI values (occurring in June) at each position then averaged the values for 2 years. We then used these LAI estimates based on the topographic positions from the two transects as estimates of LAI for the other transects where LAI was not measured.

At each sampling point, we determined the bulk density in the center of the Ap horizon using sampling rings (100 cm³, 5 cm ϕ). The soil samples were then dried at 105 °C for 24 h. The bulk density from the sediment was estimated for the horizon from 2 to 7 cm based on a sediment core taken in the center of the kettle hole (see Kleeberg et al. 2016, for further information). We calculated the C stock for the soil and sediment horizon from 2 to 7 cm by multiplying the bulk total organic carbon (TOC) content with the respective bulk density.

Bulk soil and sediment properties

As a first step, we removed the physically uncomplexed coarse organic particles (> 0.315 mm; defined as OP_{cl}) by electrostatic attraction according to Kaiser et al. (2009). The clay, silt and sand contents (fine, medium, coarse) were determined by wet-sieving and sedimentation after the destruction of OM via H_2O_2 and of carbonates via HCl following the German guideline DIN ISO 11277 (2002). The pH of “coarse- OP_{cl} -free” soil and sediment samples was measured in a 0.01 M $CaCl_2$ solution with a pH electrode following DIN ISO 10390 (1997). The effective cation exchange capacity (CEC) and the exchangeable cations Ca (Ca_{ex}) and Mg (Mg_{ex}) were analyzed via inductively coupled plasma optical emission spectroscopy (ICP-OES) with an ICP-iCAP 6300 DUO (Thermo Scientific, Bremen) after samples were treated according to DIN ISO 11260 (1994). The amount of oxalate-extractable Fe (Fe_{ox}) and Al (Al_{ox}) were determined according to (DIN 19684-6 1997) by ICP-OES, while dithionite-citrate-bicarbonate extractable Fe (Fe_{DCB}) and Al (Al_{DCB}) were measured by ICP-OES after treatment according to Schlichting et al. (1995). Total inorganic carbon (TIC) content was analyzed in ground samples using a RC612 multiphase C/N analyzer (LECO Corporation, Michigan, USA) according to DIN ISO 10694 (1995). All measurements except for the pH were conducted in duplicates. The maximum measurement uncertainties were for $Ca_{ex} < 0.34$ $cmol_c\ kg^{-1}$ (standard error), for $Mg_{ex} < 0.03$ $cmol_c\ kg^{-1}$, for $CEC < 1.22$ $cmol_c\ kg^{-1}$, for $TIC < 1.46$ $g\ kg^{-1}$, for Fe_{ox} and $Fe_{DCB} < 0.08$ $g\ kg^{-1}$, and for Al_{ox} and $Al_{DCB} < 0.02$ $g\ kg^{-1}$.

Sequential organic matter extraction

Physically uncomplexed and aggregate occluded organic particles (OP) as well as water-extractable OM (WEOM, i.e., proxy for dissolved OM) and mineral associated OM (i.e., mediated by cations) fractions can be sequentially separated from agricultural soil by combining electrostatic attraction, wet-sieving, water-extraction, ultrasonication, and $Na_4P_2O_7$ -extraction (Kaiser et al. 2009, 2010, 2012, 2016). For interactions between soil OM and minerals in agricultural soils with a near neutral pH agricultural soils (Kaiser et al. 2012), the alkaline Na-pyrophosphate extraction

procedure is supposed to separate OM interacting with polyvalent cations (Bremner et al. 1946; Masiello et al. 2004) and via polyvalent cations with soil mineral surfaces (Bremner and Lees 1949; Wattel-Koekkoek et al. 2003).

Our sequential extraction method is based on those described in: Kaiser et al. (2009, 2010, 2012). In step (1), 5 g of “coarse- OP_{cl} -free” soil and sediment samples were mixed with 50 ml of deionized water for 12 h at room temperature on a rock and roll shaker. The samples were centrifuged for 35 min at 1400 g and the supernatant was poured through two sieves (250 and 63 μm) into a beaker to obtain physically uncomplexed organic particles not separated during electrostatic attraction. Organic particles in the sieves were freeze-dried and called OP_{W1-250} and $OP_{W1-63-250}$. The decanted supernatants were vacuum-filtrated using polyamide membrane filters with a mesh size 0.45 μm (Whatman; VWR, Darmstadt, Germany), denoted as water-extractable OM ($WEOM_{free}$) and an aliquot was taken for dissolved organic carbon (DOC) and dissolved total nitrogen (DTN) analysis. Vacuum filtration prior to separation of aliquots was carried out for all the following extractions. Step (2), the solid pellet was mixed with 25 ml deionized water and sonicated with 60 $J\ ml^{-1}$ to disperse macroaggregates (MaA) (Amelung and Zech 1999). The suspension was shaken and allowed to settle for 5 min to allow organic particles to float. The supernatant was passed through two sieves (250 and 63 μm) and collected in a beaker. The solid residue was mixed with 20 ml deionized water, shaken, allowed to settle for 5 min and again passed through the sieves. This procedure was repeated two more times. Organic particles in the sieves were freeze-dried and denoted $OP_{MaA-250}$ and $OP_{MaA-63-250}$. The combined supernatants were centrifuged and decanted. The remaining solid particles in the centrifuge tube were mixed with the residuum of the first centrifugation. The decanted, vacuum-filtrated supernatants were denoted as $WEOM_{MaA}$. Step (3), the remaining solid residue was sonicated at 440 $J\ ml^{-1}$ to disperse microaggregates (Amelung and Zech 1999). Organic particles were obtained according to step (2), using a 63 μm sieve and denoted as OP_{MiA-63} . Vacuum-filtrated combined supernatants were denoted as $WEOM_{MiA}$. Step (4), the remaining pellet was washed with deionized water to extract potential remaining water-extractable OM. This OM was discarded afterward.

For step (5), the solid residuum was extracted with 50 ml of 0.1 M Na-pyrophosphate solution ($\text{Na}_4\text{P}_2\text{O}_7$; pH 9–10). The decanted supernatant was centrifuged, vacuum-filtered and denoted as NaPy-I. The solid residue from this step was extracted a second time following step (5) to extract Na-pyrophosphate-extractable OM as far as possible. The obtained vacuum-filtered supernatant was denoted as NaPy-II. Subsequently, NaPy-I and NaPy-II were combined and denoted as OM_{PYt} . In addition to an aliquot for DOC and DTN analysis, an additional aliquot was taken for the determination of polyvalent cations Fe, Al, Mg, Mn, Ca. Subsequently, the pH of the filtrate OM_{PYt} was adjusted with 1 M HCl to pH 2 and cooled in a refrigerator overnight to precipitate OM. The mixture was centrifuged to separate HCl insoluble OM that precipitated under low pH conditions (denoted as OM_{PYP}) from HCl soluble OM (denoted as OM_{PYS}). A subsample was taken from the latter. Both fractions were dialyzed against deionized water using cellulose hydrate membranes of 25–30 nm pore size (NADIR; Carlroth, Karlsruhe, Germany) until an electric conductivity of $< 4 \mu\text{S cm}^{-1}$ was observed. The solid extraction residue collected after $\text{Na}_4\text{P}_2\text{O}_7$ extraction was washed four times with deionized water, centrifuged, dialyzed, and denoted as OM_{ER} . All obtained fractions were freeze dried. All extraction steps were done in three replicates per sample.

Stable isotope analysis

Prior to $\delta^{13}\text{C}$ stable isotope analysis of the “coarse- OP_{el} -free” samples (OM_{bulk}), OM_{ER} and freeze-dried WEOM fractions, inorganic C was removed by acid fumigation according to Harris et al. (2001). For acid fumigation of the latter, no water was added because water would re-dissolve freeze-dried OM. $\delta^{13}\text{C}$ of the two OP fractions and $\delta^{15}\text{N}$ for all fractions were analyzed on samples that were not acidified. Samples were weighed into tin capsules and combusted in an elemental analyzer (Flash HT, Thermo Scientific, Bremen, Germany). Isotope ratios were measured with a Thermo-Scientific, Delta V advantage isotope ratio mass spectrometer (Bremen, Germany) coupled to an elemental analyzer. Isotopic calibration was to IAEA-CH-6 (sucrose), USGS40 (L-glutamic acid) and IAEA-N-1 (ammonium sulfate). The isotopic values are expressed in delta notation (in ‰ units), relative to VPDB (Vienna Pee Dee Belemnite) for carbon and N_2

in air for nitrogen. Analysis of internal laboratory standards ensured that the estimates of the isotopic values were precise to within $< 0.1\text{‰}$ for $\delta^{13}\text{C}$ and $< 0.5\text{‰}$ for $\delta^{15}\text{N}$.

Organic C and N contents and Na-pyrophosphate extractable cations

Total organic carbon (TOC) and total nitrogen (TN) concentrations (in wt%) of OM_{bulk} , OM_{ER} and OP fractions were measured by EA-IRMS measurements. Measurements were conducted on each fraction of a sample if enough material was available (then $n = 3$); if not, replicates were combined. The maximum uncertainty for TOC of OM_{bulk} and OM_{ER} was $< 0.46 \text{ g kg}^{-1}$ (standard error) and $< 0.08 \text{ g kg}^{-1}$ for the OP fractions. The uncertainty for TN of OM_{bulk} and OM_{ER} was $< 0.04 \text{ g kg}^{-1}$ and $< 0.01 \text{ g kg}^{-1}$ for the OP fractions. DOC and DTN of WEOM and OM_{PYt} fractions were measured using a Shimadzu TOC-Vpch after acidifying the samples with 1 M HCl to pH < 3 . Concentrations of Fe and Al in the Na-pyrophosphate extract OM_{PYt} were analyzed via ICP-OES with a ICP-iCAP 6300 DUO (Thermo Scientific, Bremen). Measurements of DOC, DTN, Fe and Al were always conducted on all replicate fractions of a sample ($n = 3$). The maximum uncertainties of DOC were $< 0.02 \text{ g kg}^{-1}$ (standard error) for the water extractable fractions and $< 0.20 \text{ g kg}^{-1}$ for the OM_{PYS} and OM_{PYP} , of TDN $< 0.01 \text{ g kg}^{-1}$ for the water extractable fractions and $< 0.02 \text{ g kg}^{-1}$ for the OM_{PYS} and OM_{PYP} . The uncertainties of Fe_{PYt} were $< 0.04 \text{ g kg}^{-1}$ for soils and of $\text{Fe}_{\text{PYt}} < 0.18 \text{ g kg}^{-1}$ for sediments, and of $\text{Al}_{\text{PYt}} < 0.02 \text{ g kg}^{-1}$ for soils and of $\text{Al}_{\text{PYt}} < 0.08 \text{ g kg}^{-1}$ for sediments.

Combination of fractions

To reduce the number of fractions discussed in this study, we combined the results of the single OM fractions that constituted less than 1.5% of total soil organic carbon (SOC). $\delta^{13}\text{C}$ and $\delta^{15}\text{N}$ of the combined fractions were calculated based on their mass. We combined the results of OP_{el} , $\text{OP}_{\text{W1-250}}$ and $\text{OP}_{\text{W1-63-250}}$ and denoted the combined fractions as OP_{free} that represented loosely bound OM susceptible to management (Table 1). Furthermore, the results of $\text{OP}_{\text{MaA-250}}$, $\text{OP}_{\text{MaA-63-250}}$ and $\text{OP}_{\text{MiA-63}}$ were combined and named OP_{A} thus representing

Table 1 Overview of the fractionation scheme and fractions discussed in this study and their ecological relevance

Step	Task	Fraction	Ecological relevance
Soil sample < 2 mm		OM _{bulk}	Combination of all fractions
Electrostatic attraction	Separation of OP > 315 μm	OP _{free}	Freely available/loosely bound OP, originating from plant production, susceptible to management, poorly decomposed
Water extraction 12 h	Separation of OP floating on water (> 250 μm, 63–250 μm; ρ < 1 g cm ⁻³)		
	Separation of water-extractable OM	WEOM _{free}	Freely available water-extractable OM, susceptible to management and erosion
Ultra-sonication 60 J ml ⁻¹	Separation of OP subsequent to macro-aggregate dispergation (> 250 μm, 63–250 μm; ρ > 1 g cm ⁻³)	OP _A	Aggregate bound OP, susceptible to management, stronger decomposed
	Separation of water-extractable OM subsequent to macro-aggregate dispergation	WEOM _A	Aggregate bound water-extractable OM, stronger decomposed and stabilized, susceptible to management and erosion
Ultra-sonication 440 J ml ⁻¹	Separation of water-extractable OM subsequent to micro-aggregate dispergation		
Na-pyrophosphate extraction followed by acidification to pH < 2	Separation of Na-pyrophosphate extractable and HCl-soluble OM	OM _{PYS}	OM bound via cation mediated interactions
	Separation of Na-pyrophosphate extractable and HCl-insoluble OM	OM _{PYP}	OM bound via cation mediated interactions, larger molecules compared to OM _{PYS}
Extraction residue		OM _{ER}	OM occluded in highly stable micro-aggregates

aggregate occluded OP released after ultra-sonication. Similarly, the results from WEOM_{MaA} and WEOM_{MiA} were combined, denoted as WEOM_A and representing aggregate protected WEOM released after ultra-sonication.

Topographic indices

Different terrain attributes and indices, such as curvature, slope and TWI were calculated from a high resolution digital elevation model (DEM) (grid-cell size 1 m × 1 m, derived by airborne laser scanning) using the geographic information system SAGA GIS (Conrad et al. 2015). To characterize the relative topographical position of points in the field compared to the neighborhood (25 m, circle) the Topographic Position Index (TPI25) was calculated using an algorithm described in Deumlich et al. (2010).

Rayleigh distillation

The Rayleigh distillation model is a way to describe isotopic dynamics of substrates over space or time. In a closed system, there is a lack of new inputs leading to a progressive conversion of the initial substrate (Fry 2006). During the reaction and with decreasing mass

of the initial substrate an isotopic change in the remaining substrate occurs. In this case, the relationship between the isotopic ratios in the remaining substrate and the reacted fraction of the substrate is described with an exponential model. However, in an open system new substrate with a potentially different isotopic composition is added continually as the initial substrate changes simultaneously (Fry 2006). In our case, we assumed an open system in which new OM inputs are introduced by plant production or slurry and by the transport of organic particles or OM attached to mineral surfaces from higher topographic positions (Fig. 1). Losses of OM at each topographic position occur through transport and microbial decomposition of OM. As such, we do not interpret the results of a Rayleigh model strictly in terms of isotopic fractionation, but we use it as a conceptual model (sensu Cohen 2003) to infer different OM sources and transport gains or losses at the spatial scale of the transect. In this case, the relationship between the isotopic values and the log transformation of elemental (C or N) concentration of each fraction are graphically represented. In this analysis, we consider the slope of the Rayleigh model to integrate spatial (e.g. erosion, transfer) and temporal (e.g., inputs and microbial decomposition) effects that describe the

landscape impact on OM turnover. Thus, a comparison of Rayleigh model slopes allows for testing for different rates of “transformation” among the different stabilized OM fractions, i.e., low slopes indicate a slow turnover, while steep slopes indicate a fast turnover.

Statistical analysis

We used the Shapiro–Wilk test to test for normally distributed data. We used analysis of variance (ANOVA) to test for differences in soil chemical and mineral characteristics, $\delta^{13}\text{C}$ and $\delta^{15}\text{N}$ isotope signatures, OC contents and molar C:N ratios between topographic positions and OM fractions using R (version 3.1.1, R Foundation for Statistical Computing, Vienna, Austria, <http://www.R-project.org/>). We performed Tukey’s HSD post hoc test to identify these differences. To explore relationships of $\delta^{13}\text{C}$, $\delta^{15}\text{N}$ and OC content with soil chemical and mineral characteristics we used Pearson product-moment correlation analyses when the data were normally distributed and Spearman rank order correlation analyses for non-normally distributed data. Correlation coefficients were considered to be significant at the $p \leq 0.05$ level. In order to test for relationships of $\delta^{13}\text{C}$, $\delta^{15}\text{N}$ and OC contents with catchment characteristics and plant productivity, we performed a linear mixed effects model (LME; R package nlme Kuznetsova et al. 2016). Here, we used TWI, TPI25, elevation, curvature, slope, LAI and interactions among them as continuous fixed effect variables, where the transects and fractions were considered random effect variables while nesting fractions in transects: $\text{lme}(y \sim \text{curvature} + \text{slope} + \text{elevation} + \text{TWI} + \text{TPI25} + \text{LAI}$,

random ~ 1 transect/fraction). To identify the most parsimonious model including only significant predictor variables for each explanatory variable, we used a step-wise ANOVA approach based on the Akaike information criterion (AIC) to achieve an optimal model that explains the most variation with the fewest variables. We used ANOVA to compare slopes of the Na-pyrophosphate extracted OM (OM_{PYS} , OM_{PYP}), OM_{ER} , and OM in the aggregate fractions.

Results

Pattern of topographic indices and leaf area index

We found the largest mean curvature at hilltops with $0.6 \pm 0.1^\circ$ ($n = 4$; mean \pm standard error) and the smallest curvature at footslopes with $-0.1 \pm 0.1^\circ$ (Table 2). The steepest slope was found at hillslopes with a mean of $5.7 \pm 0.4^\circ$. While the TWI was similar between hilltops (4.8 ± 0.5) and hillslopes (5.0 ± 0.3), it was significantly higher for footslopes (8.9 ± 0.8) and edges (8.7 ± 0.4) ($p < 0.01$). We found that data were usually normally distributed with very few exceptions. The significantly highest TPI25 was found for hilltops (0.6 ± 0.1) and the lowest TPI25 for footslopes (-0.3 ± 0.0). LAI increased toward the kettle hole from only 2.8 ± 0.3 at hilltops to 4.9 ± 0.3 at edges.

Soil and sediment chemical and mineral characteristics

Clay content in the catchment was greatest at hillslopes ($145 \pm 12 \text{ g kg}^{-1}$) and smallest at edges

Table 2 Topographic indices of soil sampling locations (mean \pm standard error)

Landscape position	Distance [#] (m)	Elevation (m.a.s.l.)	Curvature ($^\circ$)	Slope ($^\circ$)	TWI	TPI25	LAI [§]
Hilltop	42.0 ± 3.0	91.5 ± 0.6	0.6 ± 0.1^a	2.9 ± 1.0^a	4.8 ± 0.5^a	0.6 ± 0.1	2.8 ± 0.3
Hillslope	27.1 ± 1.6	90.3 ± 0.4	$0.2 \pm 0.1^{a,b}$	5.7 ± 0.4	5.0 ± 0.3^a	0.2 ± 0.1^b	3.9 ± 0.4
Footslope	10.1 ± 2.0	88.8 ± 0.1	-0.1 ± 0.1^b	2.3 ± 0.4^a	8.9 ± 0.8^b	-0.3 ± 0.0^a	4.9 ± 0.5
Edge	2.0 ± 0.3	88.6 ± 0.1	$0.1 \pm 0.2^{a,b}$	2.4 ± 0.6^a	8.7 ± 0.4^b	$-0.1 \pm 0.1^{a,b}$	4.9 ± 0.3

TPI25 topographic position index, TWI topographic wetness index, LAI leaf area index

[#]Horizontal distance

[§] $n = 8$

^{a,b}Landscape positions, which are not significantly different from each other according to the Tukey’s HSD post hoc test ($p \leq 0.05$ level) share the same letter. We do not report estimates of significance (p values) for LAI due to the low number of replicates per each topographic position ($n = 2$)

Table 3 Clay, silt, total inorganic carbon (TIC) contents, cation exchange capacity (CEC), amounts of exchangeable Ca (Ca_{ex}) and Mg (Mg_{ex}), and pH of each ($n = 4$) sampling location (mean \pm standard error)

Landscape position	Density ($g\ cm^{-3}$)	Clay ($g\ kg^{-1}$)	Silt	pH	TIC ($g\ kg^{-1}$)	CEC ($cmol_c\ kg^{-1}$)	Ca_{ex} ($cmol_c\ kg^{-1}$)	Mg_{ex} ($cmol_c\ kg^{-1}$)
Hilltop	$1.73 \pm 0.02^{\S}$	135 ± 15^a	238 ± 19^a	7.6 ± 0.0^a	7.20 ± 1.97^a	9.32 ± 1.17^a	10.60 ± 0.99^a	0.45 ± 0.05^a
Hillslope	$1.69 \pm 0.02^{\S}$	145 ± 12^a	248 ± 3^a	$7.2 \pm 0.0^{a,b}$	4.06 ± 2.82^a	9.00 ± 0.71^a	9.35 ± 0.63^a	$1.03 \pm 0.24^{a,b}$
Footslope	1.56^{\ddagger}	90 ± 16^b	243 ± 6^a	$6.9 \pm 0.2^{a,b}$	2.19 ± 1.05^a	7.47 ± 1.01^a	7.00 ± 1.37^a	$1.26 \pm 0.29^{a,b}$
Edge	$1.62 \pm 0.01^{\S}$	73 ± 15^a	260 ± 11^a	6.4 ± 0.4^b	1.35 ± 0.25^a	7.00 ± 1.61^a	6.28 ± 1.47^a	$0.96 \pm 0.15^{a,b}$
Kettle hole	2.42^*	$328 \pm 49^{\S}$	$620 \pm 9^{\S}$	$7.1 \pm 0.1^{\S}$	2.72 ± 0.24^a	23.57 ± 1.19	23.96 ± 1.72	1.61 ± 0.39^b

$^{\S}n = 2$

$^{\ddagger}n = 1$

*Based on results from Kleeberg et al. (2016)

a,b Landscape positions, which are not significantly different from each other according to the Tukey's HSD post hoc test ($p \leq 0.05$ level) share the same letter

($73 \pm 15\ g\ kg^{-1}$) (Table 3). Kettle hole sediments had much greater clay contents than the soil ($328 \pm 49\ g\ kg^{-1}$, $n = 2$), but contained almost no sand ($52 \pm 39\ g\ kg^{-1}$). The pH decreased toward the kettle hole with 7.6 ± 0.0 at hilltops being significantly higher compared to edges with a mean of 6.4 ± 0.4 ($p = 0.03$) as does TIC with $7.20 \pm 1.97\ g\ kg^{-1}$ at hilltops to $1.35 \pm 0.25\ g\ kg^{-1}$ at edges. Similarly, the CEC decreased from $9.32 \pm 1.17\ cmol_c\ kg^{-1}$ at hilltops to $7.00 \pm 1.61\ cmol_c\ kg^{-1}$ at edges and Ca_{ex} patterns were similar, while Mg_{ex} increased toward the kettle hole with the content of Mg_{ex} being significantly lower at hilltops compared to the kettle hole ($p = 0.04$). The CEC was significantly higher in kettle hole sediments compared to soils with $23.57 \pm 1.19\ cmol_c\ kg^{-1}$, similar patterns were also found for Ca_{ex} ($p < 0.01$). As such, Ca_{ex} largely explained the CEC patterns. The content of Fe_{DCB} was larger in the erosional areas compared to depositional areas and the largest content was found in sediments ($8.42 \pm 1.15\ g\ kg^{-1}$) (Fig. 3). The concentration of Fe_{ox} was smaller than Fe_{DCB} , but increased from $0.96 \pm 0.12\ g\ kg^{-1}$ at hilltops to $1.26 \pm 0.6\ g\ kg^{-1}$ at edges and were almost four times higher in sediments ($5.58 \pm 0.52\ g\ kg^{-1}$) ($p < 0.01$). As such, the ratio of $Fe_{ox}:Fe_{DCB}$ decreased with topographic position and distance from the kettle hole shoreline. Fe_{PYt} contents were again significantly lower than those of Fe_{ox} ($p < 0.01$), but followed the same pattern. Correspondingly, the ratio of $Fe_{PYt}:Fe_{DCB}$ was even lower than of $Fe_{ox}:Fe_{DCB}$, but decreased with topographic position. Similar to the contents of extractable Fe, the Al contents decreased from $Al_{DCB} > Al_{ox} > Al_{PYt}$, whereas Al_{PYt} increased with topographic position.

Organic carbon

The OM_{bulk} average OC stock increased toward the kettle hole (Fig. 4). Similarly, mean OC contents across all fractions were found to increase from hilltops to the kettle hole edge and were highest in the kettle hole sediments (Table 4), however their percentage of SOC varied depending on the fraction (Fig. 4). Overall, we found OC contents of nearly all fractions from the kettle hole sediment, except for OP fractions, to be significantly larger compared to the OC contents from the soils ($p < 0.01$). While the OC

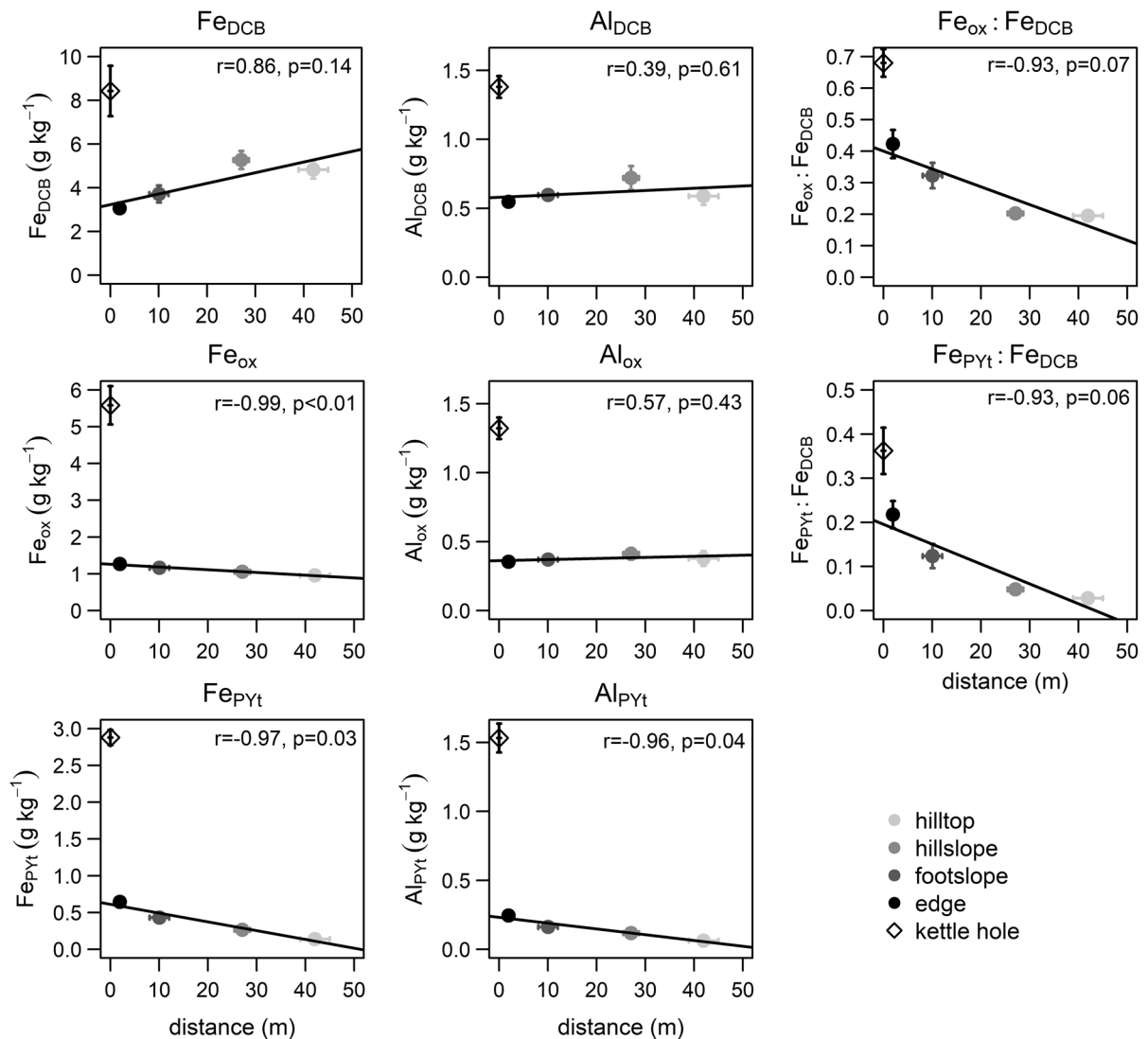


Fig. 3 Contents of the dithionite-citrate-bicarbonate extractable Fe (Fe_{PYt}) and Al (Al_{DCB}), oxalate extractable Fe (Fe_{ox}) and Al (Al_{ox}), Na-pyrophosphate extractable Fe (Fe_{PYt}) and Al (Al_{PYt}), and the ratios of $Fe_{ox} : Fe_{DCB}$ and $Fe_{PYt} : Fe_{DCB}$ versus the distance of the sampling position to the kettle hole shoreline (m). The black solid lines represent regressions lines

through the four topographic positions in the catchment with the correlation coefficient r . Pearson correlation coefficients (r) are reported for each regression. Kettle hole values are presented as reference and are not included in the regression, thus the distance from the shoreline is not reported

made up by the sum of OP_{free} and OP_A were on average $5.9 \pm 0.5\%$ of SOC at hilltops, their proportion was with 12.5 ± 1.1 and $11.0 \pm 0.5\%$ significantly greater at footslopes and edges, respectively ($p < 0.01$). OC contents in OP_{free} and OP_A from sediments was again significantly larger and made up $22.8 \pm 8.0\%$ of SOC ($p < 0.01$), though having a large range from 4.7 to 44.4% among the four samples

with $> 90\%$ OC from OP found in OP_A . Accordingly, all other sediment fractions varied greatly in percentage of SOC across the four replicate samples. The proportion of $WEOM_{free}$ was small ranging on average from 1.2 ± 0.0 to $1.5 \pm 0.1\%$ depending on topographic position, while $WEOM_A$ made up 2.6 ± 0.1 to $3.9 \pm 0.3\%$ of total SOC, except for sediments where it was only $1.7 \pm 0.3\%$. The proportion of OM_{PYt}

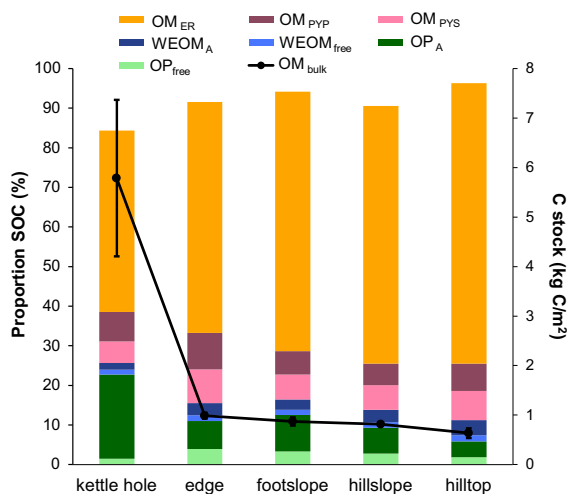


Fig. 4 Proportion of organic carbon contents of organic matter (OM) fractions (in wt%) with respect to the total soil organic carbon (SOC) for the topographic positions ($n = 4$ per position). We attribute the differences of the recovery rates from 100% to losses during vacuum filtration. Black points connected by solid black lines represent the C stocks (in kg C m^{-2}) of the horizon from 2 to 7 cm. OM_{bulk} organic matter in the bulk soil, OP_{free} loosely bound organic particles, OP_{A} aggregate occluded organic particles, $WEOM_{\text{free}}$ loosely attached water-extractable organic matter, $WEOM_{\text{A}}$ aggregate-bound water-extractable organic matter, OM_{PYS} Na-pyrophosphate extractable and HCl-soluble organic matter, OM_{PYP} Na-pyrophosphate extractable and HCl-insoluble organic matter, OM_{ER} organic matter in the extraction residue

ranged from $12.9 \pm 2.2\%$ in sediments to $17.8 \pm 1.4\%$ at the edges. The largest proportion of OC was left in OM_{ER} , where it averaged to $45.8 \pm 6.3\%$ in sediments and reaching up to $70.8 \pm 2.0\%$ at hilltops. Therefore, stable isotope values of OM_{bulk} are dominated by the mineral-associated fractions (OM_{PYS} , OM_{PYP} , OM_{ER}). The sum of our fractions was less than 100% of total SOC, we assume this was a result from measurement uncertainties and OM attached to mineral particles larger than $0.45 \mu\text{m}$, which were lost during vacuum filtration.

$\delta^{13}\text{C}$, $\delta^{15}\text{N}$, and C:N ratio patterns

$\delta^{13}\text{C}$ values of OM_{bulk} from soils gradually decreased from hilltops toward the kettle hole with $-26.5 \pm 0.1\text{‰}$ to edges with $-27.8 \pm 0.2\text{‰}$ (Fig. 5). OM_{bulk} from the kettle hole sediments was depleted in ^{13}C with $\delta^{13}\text{C} = -28.5 \pm 0.3\text{‰}$ compared to the soils. $\delta^{13}\text{C}$ of OP fractions, OM_{PY}

fractions, and OM_{ER} fell along the Rayleigh distillation line. The same fractions from the kettle holes sediments were often more depleted in ^{13}C than the edge sample, following the Rayleigh trend, but the OC contents were substantially higher than the linear trend of the soil samples. The slopes of the linear relationships of soil samples between the $\delta^{13}\text{C}$ values and the log-transformed OC content were negative for most fractions ranging from -5.5 (OM_{ER}) to -2.8 (OM_{PYP}). Generally, OM_{PYS} from hilltops was significantly enriched in ^{13}C with $\delta^{13}\text{C} = -26.0 \pm 0.1\text{‰}$ ($p = 0.01$) and OP_{A} from the kettle hole was significantly depleted in ^{13}C with $\delta^{13}\text{C} = -29.1 \pm 0.2\text{‰}$ ($p < 0.01$) (Table 4). OM_{PYS} was always found to be more enriched in ^{13}C than OM_{PYP} . Interestingly, $WEOM_{\text{free}}$ and $WEOM_{\text{A}}$ showed a different pattern; in fact, $WEOM_{\text{A}}$ from edges was even significantly enriched in ^{13}C compared to the other topographic positions ($p < 0.01$) and had a positive slope.

The slopes of the Rayleigh models for the two OM_{PY} fractions were significantly different ($p < 0.01$), although, the slopes of the OM_{PYP} and both OM_{OP} fractions were not significantly different at the $\alpha = 0.05$ level. In addition, the OM_{ER} Rayleigh slope was not significantly different from the OM_{PYS} fraction, thus resulting in two groups of OM turnover: the OM_{ER} and OM_{PYS} in one, and the OM_{PYP} , OP_{free} , and OP_{A} in the other.

In contrast to soils, OP_{free} in sediments was significantly enriched in ^{13}C than OP_{A} ($p < 0.01$). $WEOM_{\text{A}}$ from footslopes and edges was significantly enriched in ^{13}C compared to $WEOM_{\text{free}}$ ($p < 0.01$) at the same positions. The $\delta^{13}\text{C}$ of both fractions was in the same range at hilltops and hillslopes. In contrast, $WEOM_{\text{A}}$ of the kettle hole sediment was significantly depleted in ^{13}C than $WEOM_{\text{free}}$ ($p < 0.01$). While OM_{PYS} , OM_{PYP} and OM_{ER} from hilltops, hillslopes, and footslopes were consistently more enriched in ^{13}C than $WEOM_{\text{free}}$ and $WEOM_{\text{A}}$ ($p < 0.01$; except for OM_{PYP} from footslopes), the same fractions were in similar range to kettle hole sediments.

$\delta^{15}\text{N}$ values of OM_{bulk} did not show any clear trend but footslopes were found to be significantly enriched with $\delta^{15}\text{N} = 6.2 \pm 0.3\text{‰}$ and kettle hole sediments were significantly depleted with $\delta^{15}\text{N} = 3.4 \pm 0.4\text{‰}$ ($p < 0.01$) (Fig. 6; Table 4). In general, sediment fractions were consistently depleted in ^{15}N except for $WEOM_{\text{free}}$. OP_{free} , OP_{A} and OM_{ER} were consistently significantly enriched at footslopes ($p < 0.01$).

Table 4 Mean organic carbon (OC) contents and below in brackets their percentage of soil organic carbon, $\delta^{13}\text{C}$ and $\delta^{15}\text{N}$ and molar C:N ratio \pm standard errors of the different fractions for each landscape position

Variable	Landscape position	OM _{bulk}	OP _{free}	OP _A	WEOM _{free}	WEOM _A	OM _{PYS}	OM _{PYP}	OM _{ER}	
OC (g kg ⁻¹ soil)	Hilltop	7.36 ± 0.66 ^a	0.14 ± 0.01 ^a (1.9 ± 0.2)	0.29 ± 0.04 ^a (3.9 ± 0.4)	0.11 ± 0.01 ^a (1.5 ± 0.1)	0.23 ± 0.01 ^a (5.4 ± 0.3)	0.54 ± 0.03 ^a (7.3 ± 0.3)	0.51 ± 0.04 ^a (7.4 ± 0.3)	5.19 ± 0.45 ^a (70.8 ± 2.0)	
	Hillslope	9.63 ± 0.97 ^a	0.25 ± 0.06 ^a (2.8 ± 0.9)	0.61 ± 0.08 ^a (6.5 ± 0.7)	0.13 ± 0.01 ^a (1.4 ± 0.1)	0.25 ± 0.01 ^a (4.6 ± 0.3)	0.59 ± 0.03 ^a (6.2 ± 0.4)	0.52 ± 0.04 ^a (5.0 ± 0.3)	6.28 ± 0.69 ^a (65.1 ± 1.9)	
	Footslope	11.13 ± 0.19 ^a	0.37 ± 0.08 ^a (3.4 ± 0.7)	1.02 ± 0.08 ^a (9.1 ± 0.6)	0.15 ± 0.00 ^a (1.3 ± 0.0)	0.24 ± 0.02 ^a (4.0 ± 0.1)	0.70 ± 0.02 ^{a,b} (6.3 ± 0.3)	0.66 ± 0.02 ^a (5.4 ± 0.2)	7.30 ± 0.30 ^a (65.5 ± 2.1)	
	Edge	12.24 ± 1.22 ^a	0.49 ± 0.01 ^a (4.0 ± 0.5)	0.86 ± 0.05 ^a (7.1 ± 0.2)	0.18 ± 0.01 ^a (1.5 ± 0.1)	0.29 ± 0.02 ^a (4.5 ± 0.2)	1.03 ± 0.05 ^a (8.6 ± 0.5)	1.10 ± 0.05 ^a (9.2 ± 0.9)	7.15 ± 0.75 ^a (58.3 ± 1.0)	
	Kettle hole		47.48 ± 13.05	0.96 ± 0.65 ^a (1.5 ± 0.7)	13.27 ± 7.30 ^a (21.8 ± 8.0)	0.50 ± 0.04 (1.2 ± 0.2)	0.61 ± 0.08 (1.7 ± 0.3)	2.21 ± 0.19 (5.4 ± 1.0)	3.14 ± 0.39 (7.5 ± 1.3)	19.47 ± 2.57 (45.8 ± 6.3)
$\delta^{13}\text{C}$ (‰)	Hilltop	-26.5 ± 0.1 ^a	-27.0 ± 0.4 ^a	-26.8 ± 0.1	-28.4 ± 0.2 ^a	-28.0 ± 0.0 ^a	-26.0 ± 0.1 ^a	-27.0 ± 0.1 ^a	-26.7 ± 0.1 ^a	
	Hillslope	-26.7 ± 0.1 ^a	-27.9 ± 0.1 ^{a,b}	-27.8 ± 0.2 ^a	-28.4 ± 0.2 ^a	-28.1 ± 0.1 ^a	-26.3 ± 0.1 ^a	-27.5 ± 0.2 ^{a,b}	-27.0 ± 0.1 ^{a,b}	
	Footslope	-27.0 ± 0.2 ^{a,c}	-28.2 ± 0.3 ^{a,b}	-28.3 ± 0.1 ^{a,b}	-28.4 ± 0.3 ^a	-27.7 ± 0.1 ^{a,b}	-26.5 ± 0.0 ^a	-27.7 ± 0.1 ^b	-27.3 ± 0.1 ^{a,b}	
	Edge	-27.8 ± 0.2 ^{b,c}	-28.7 ± 0.2 ^b	-28.9 ± 0.1 ^{b,c}	-28.4 ± 0.2 ^a	-27.3 ± 0.1 ^b	-27.3 ± 0.2 ^b	-28.1 ± 0.1 ^{b,c}	-27.8 ± 0.1 ^{b,c}	
	Kettle hole		-28.5 ± 0.3 ^b	-27.9 ± 0.6 ^{a,b}	-29.1 ± 0.2 ^c	-28.0 ± 0.3 ^a	-28.6 ± 0.2	-27.3 ± 0.3 ^b	-28.8 ± 0.3 ^c	-28.7 ± 0.4 ^c
$\delta^{15}\text{N}$ (‰)	Hilltop	5.6 ± 0.2 ^a	3.9 ± 0.4 ^{a,b}	3.6 ± 0.2 ^{a,b}	3.3 ± 0.3 ^a	3.7 ± 0.4 ^{a,b}	5.8 ± 0.2 ^a	5.8 ± 0.3 ^a	5.7 ± 0.2 ^a	
	Hillslope	5.3 ± 0.2 ^a	5.0 ± 0.6 ^{a,b}	3.4 ± 0.2 ^{a,b}	3.6 ± 0.1 ^a	4.0 ± 0.2 ^a	5.2 ± 0.3 ^{a,b}	5.0 ± 0.2 ^a	5.5 ± 0.3 ^a	
	Footslope	6.2 ± 0.3 ^a	6.0 ± 0.7 ^a	4.6 ± 0.5 ^a	5.1 ± 0.2 ^b	6.0 ± 0.2 ^c	5.3 ± 0.1 ^{a,b}	4.8 ± 0.2 ^a	6.1 ± 0.3 ^a	
	Edge	5.0 ± 0.3 ^a	3.7 ± 0.6 ^{a,b}	3.3 ± 0.4 ^{a,b}	5.4 ± 0.3 ^b	6.7 ± 0.1 ^c	4.4 ± 0.3 ^{b,c}	3.3 ± 0.5	5.4 ± 0.2 ^a	
	Kettle hole		3.5 ± 0.4	2.7 ± 0.4 ^b	2.7 ± 0.2 ^b	3.5 ± 0.3 ^a	2.8 ± 0.2 ^b	3.6 ± 0.3 ^c	1.9 ± 0.1	3.6 ± 0.3
C:N	Hilltop	10.2 ± 0.3 ^{a,b}	20.1 ± 1.2 ^a	15.0 ± 1.8 ^a	4.0 ± 0.3 ^{a,b}	6.2 ± 0.1 ^a	11.5 ± 0.4 ^a	15.7 ± 0.7 ^b	7.9 ± 0.6 ^a	
	Hillslope	9.9 ± 0.2 ^a	16.5 ± 2.0 ^a	16.2 ± 0.9 ^a	3.2 ± 0.4 ^a	6.0 ± 0.1 ^a	11.3 ± 0.4 ^a	12.6 ± 0.5 ^a	7.7 ± 0.4 ^a	
	Footslope	11.1 ± 0.3 ^{a,b}	17.0 ± 1.0 ^a	17.8 ± 0.6 ^a	3.2 ± 0.3 ^a	6.6 ± 0.1 ^a	11.4 ± 0.4 ^a	11.8 ± 0.3 ^a	8.2 ± 0.2 ^a	
	Edge	10.2 ± 0.1 ^{a,b}	17.1 ± 1.5 ^a	16.7 ± 0.7 ^a	5.3 ± 0.2 ^{b,c}	7.7 ± 0.3	15.5 ± 0.2	12.7 ± 0.5 ^b	8.5 ± 1.0 ^a	
	Kettle hole		11.7 ± 0.8 ^b	17.0 ± 2.0 ^a	16.5 ± 0.6 ^a	6.8 ± 0.5 ^c	6.5 ± 0.1 ^a	12.1 ± 0.2 ^a	13.7 ± 0.1 ^{a,b}	6.9 ± 0.5 ^a

OM_{bulk} organic matter in the bulk soil, OP_{free} loosely bound organic particles, OP_A aggregate occluded organic particles, WEOM_{free} loosely attached water-extractable organic matter, WEOM_A aggregate-bound water-extractable organic matter, OM_{PYS} Na-pyrophosphate extractable and HCl-soluble organic matter, OM_{PYP} Na-pyrophosphate extractable and HCl-insoluble organic matter, OM_{ER} organic matter in the extraction residue

^{a,b,c}Landscape positions, which are not significantly different from each other according to the Tukey's HSD post hoc test ($p \leq 0.05$ level), share the same letter

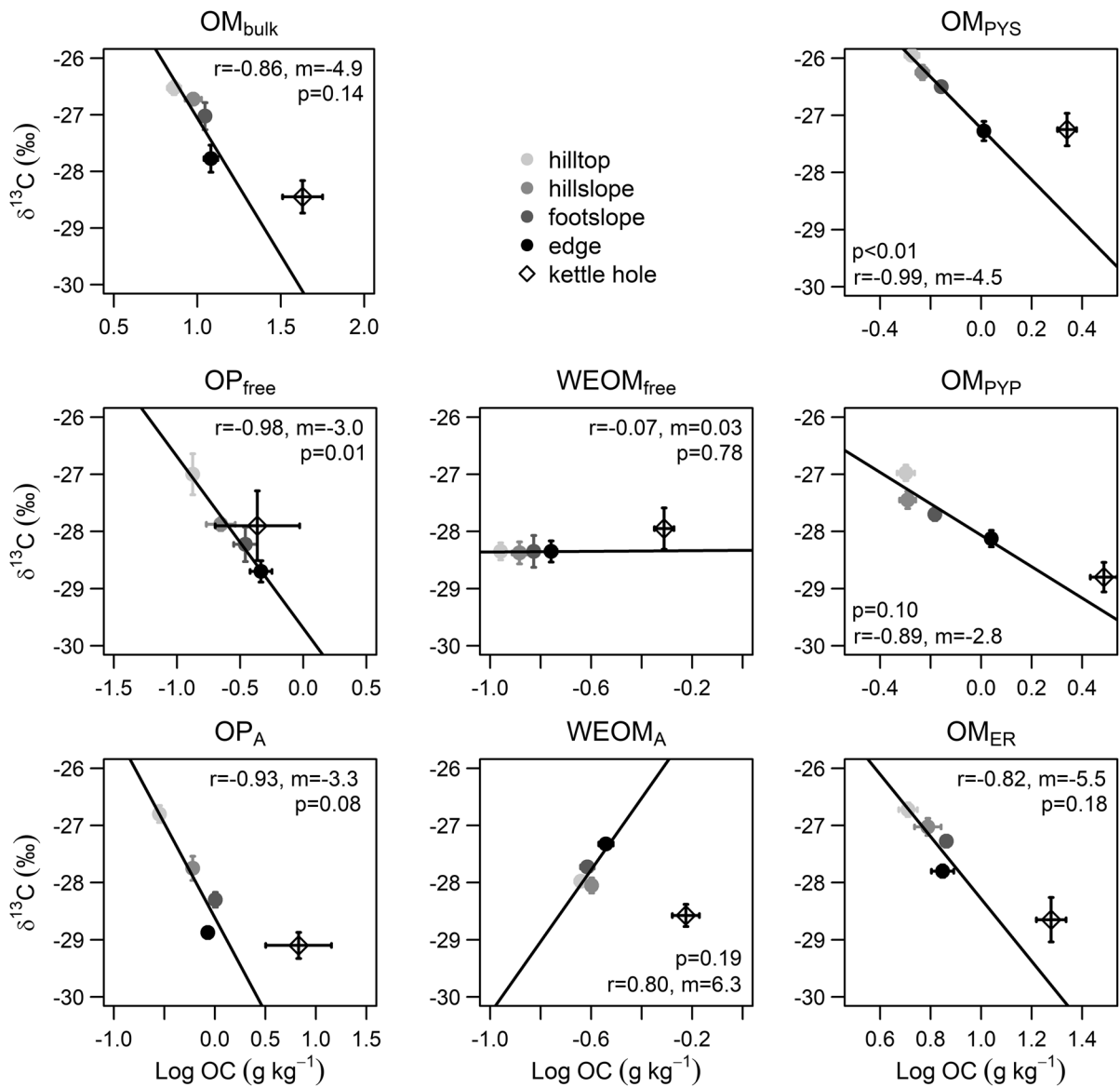


Fig. 5 Plot of $\delta^{13}\text{C}$ versus the logarithm in base 10 of the organic carbon (OC) concentration in the form of a Rayleigh distillation model for each fraction for each topographic position ($n = 4$ per position). The black solid lines represent linear regressions through the four topographic positions in the catchment with the correlation coefficient r and slope m . The p values represent the goodness of the fit. OM_{bulk} organic matter

in the bulk soil, OP_{free} loosely bound organic particles, OP_A aggregate occluded organic particles, $\text{WEOM}_{\text{free}}$ loosely attached water-extractable organic matter, WEOM_A aggregate-bound water-extractable organic matter, OM_{PYS} Na-pyrophosphate extractable and HCl-soluble organic matter, OM_{PYP} Na-pyrophosphate extractable and HCl-insoluble organic matter, OM_{ER} organic matter in the extraction residue

Footslopes aside, $\delta^{15}\text{N}$ of OP_A and OM_{ER} decreased towards the kettle hole. In fact, only $\delta^{15}\text{N}$ of OM_{PYS} and OM_{PYP} decreased towards the kettle hole. Similarly to $\delta^{13}\text{C}$, $\text{WEOM}_{\text{free}}$ and WEOM_A were increasingly enriched in ^{15}N toward the kettle hole

($p < 0.01$). The Rayleigh model slopes of the OP and OM_{ER} fractions were not significant, we therefore only compared the slopes of the OM_{PYP} and OM_{PYS} fractions: the OM_{PYP} was significantly lower ($p < 0.10$) than the OM_{PYS} .

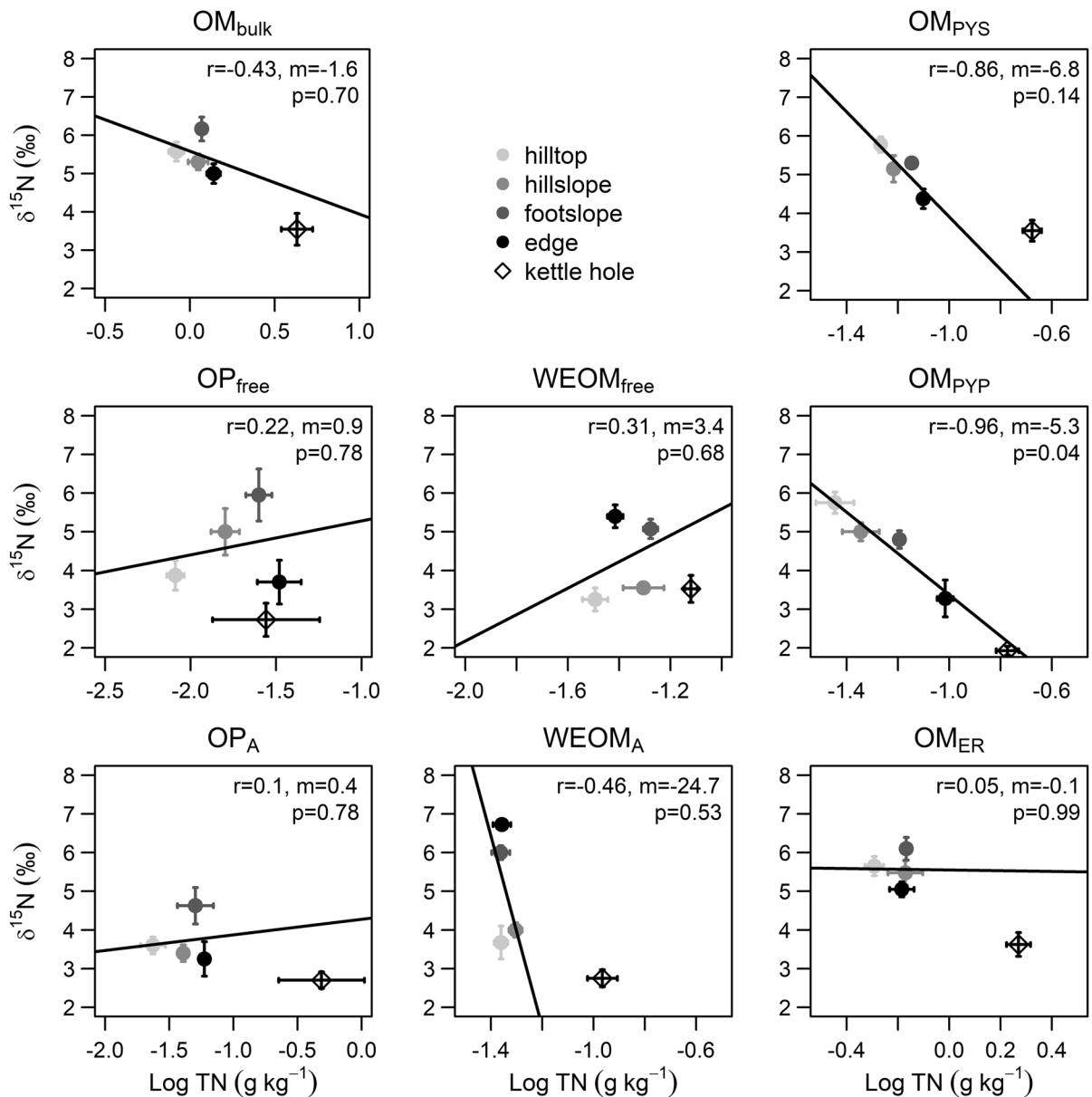


Fig. 6 Plot of $\delta^{15}\text{N}$ versus the logarithm in the base of 10 of the total nitrogen (TN) concentration based in the form of a Rayleigh distillation model for each fraction for each topographic position ($n = 4$ per position). The solid black lines represent linear regressions through the four topographic positions in the catchment with the correlation coefficient r and slope m . The p values represent the goodness of the fit. OM_{bulk} organic matter in the bulk soil, OP_{free} loosely bound

organic particles, OP_A aggregate occluded organic particles, $WEOM_{free}$ loosely attached water-extractable organic matter, $WEOM_A$ aggregate-bound water-extractable organic matter, OM_{PYS} Na-pyrophosphate extractable and HCl-soluble organic matter, OM_{PYP} Na-pyrophosphate extractable and HCl-insoluble organic matter, OM_{ER} organic matter in the extraction residue

Similar to $\delta^{13}\text{C}$, $WEOM_{free}$ of sediments was significantly enriched in ^{15}N compared to $WEOM_A$ ($p < 0.01$), whereas the opposite was observed for the other topographic positions. Furthermore, OM_{PYP} was

significantly depleted in ^{15}N to OM_{PYS} ($p < 0.01$), which was also the case for edges and footslopes, but with a lower difference between both fractions.

There was no particular pattern in molar C:N ratio of OM_{bulk} or any OM fractions visible with landscape position (Table 4). Molar C:N ratios of OM_{bulk} ranged from a mean of 9.9 ± 0.2 at hillslopes to 11.7 ± 0.8 in kettle hole sediments. The highest molar C:N ratios were found in OP_{free} and OP_A ranging from on average 15.0 ± 1.8 to 20.1 ± 1.2 at hilltops. The lowest C:N ratios were detected in $WEOM_{\text{free}}$ and $WEOM_A$ ranging between 3.2 ± 0.4 and 7.7 ± 0.3 . Molar C:N ratios from OM_{PYS} and OM_{PYP} were higher and ranged from 11.3 ± 0.4 to 15.7 ± 0.7 . Molar C:N ratios from OM_{ER} were always significantly lower than OM_{bulk} ($p < 0.01$) and ranged from 6.9 ± 0.5 to 8.5 ± 1.0 .

Linear mixed effects model

The LME results revealed that TPI25 and curvature had the most significant effect on the OC content (Table 5). With respect to $\delta^{13}\text{C}$, strong significant effects could also be observed for LAI, TPI and the interaction term between LAI, TPI25, and curvature. Elevation and curvature were found to have the largest affect on $\delta^{15}\text{N}$.

Correlation analyses of organic carbon content, $\delta^{13}\text{C}$ and $\delta^{15}\text{N}$ with soil characteristics

There were positive correlations ($r > 0.8$, $n = 16$) between OC contents of OM_{PYS} and OM_{PYP} with Fe_{PYt} and Al_{PYt} (Table 6). Positive correlations were also found between OC in OM_{PYS} and OM_{PYP} with Fe_{ox} , but the correlation coefficients were not as strong. Negative correlations could be observed for

OC in OM_{PYS} and OM_{PYP} with the content of clay-sized particles and Ca_{ex} .

Discussion

From the hilltop to kettle hole, we observed distinct patterns in the physical and chemical properties of the soil and sediment. The relatively high clay content at the hilltop position indicates that tillage has exposed the clay rich Bt horizon, and is clear evidence of the history of erosion across the site. Clay and silt contents were greatest in the kettle hole sediments highlighting the importance of the transport of terrestrial material into the kettle hole over time. The transport of soil along the transect resulted in an increase of poorly crystalline Fe and Al (oxy)hydroxides and complexed cations toward the kettle hole as these are prone to a lateral transport due to their small size (Berhe et al. 2012). Similar patterns were previously found by Ellerbrock et al. (2016) for a nearby catchment. As a result of this transport, the OC content increased along the transect from hilltop to edge, which corresponded to the landscape curvature and TPI25. The C stock was especially large in the kettle hole, emphasizing the depositional nature of these water bodies. Thus, the drivers of OM distribution across the hillslope and into the kettle hole span the transect to aggregate scales while the different OM stabilization mechanisms and OM sources are dependent on a combination of plant production, transport of material, and soil chemical properties.

Table 5 Results of the linear mixed effects (LME) model on organic carbon (OC) content and stable isotope ratios as explanatory variables

Explanatory variable	Predictor variable	Estimate	SE	t value	p value
OC	Curvature	− 2368.70	499.69	− 4.74	< 0.01
	TPI25	996.42	385.46	2.69	0.01
$\delta^{13}\text{C}$	LAI	− 0.59	0.13	− 4.58	< 0.01
	TPI25	− 0.82	0.38	− 2.17	0.03
	LAI:TPI25: Curvature	0.24	0.10	2.45	0.02
$\delta^{15}\text{N}$	Elevation	0.20	0.10	2.06	0.04
	Curvature	− 1.16	0.28	− 4.10	< 0.01

TPI25 topographic position index, LAI leaf area index

Table 6 Correlation coefficients (Pearson for normally distributed data and Spearman rank for non-normally distributed data, the latter indicated by an asterisk) between the organiccarbon (OC) content, $\delta^{13}\text{C}$ and $\delta^{15}\text{N}$ and soil characteristic including all topographic positions and transects (n = 16)

Soil characteristic	OC			$\delta^{13}\text{C}$			$\delta^{15}\text{N}$		
	OM _{PYS}	OM _{PYP}	OM _{ER}	OM _{PYS}	OM _{PYP}	OM _{ER}	OM _{PYS}	OM _{PYP}	OM _{ER}
Clay	− 0.69*	− 0.67*	ns	0.58	0.62	0.7	0.42	0.43	ns
Fe _{DCB}	− 0.60*	− 0.62*	ns	0.61	0.55	0.62	ns	0.43	ns
Fe _{ox}	0.60*	0.57*	ns	− 0.56	− 0.63	− 0.68	− 0.52	− 0.6	− 0.42
Fe _{PYT}	0.91*	0.89*	0.46	− 0.80	− 0.89	− 0.98	− 0.74	− 0.79	− 0.50
Al _{DCB}	ns	ns	ns	ns	ns	ns	ns	ns	ns
Al _{ox}	ns	ns	ns	ns	ns	ns	ns	ns	− 0.47
Al _{PYT}	0.87*	0.84*	0.41	− 0.69	− 0.84	− 0.90	− 0.78	− 0.72	− 0.56
Ca _{ex}	− 0.54*	− 0.53*	ns	0.49	0.66	0.74	0.44	ns	ns

OM_{bulk} organic matter in the bulk soil, OP_{free} loosely bound organic particles, OP_A aggregate occluded organic particles, WEOM_{free} loosely attached water-extractable organic matter, WEOM_A aggregate-bound water-extractable organic matter, OM_{PYS} Na-pyrophosphate extractable and HCl-soluble organic matter, OM_{PYP} Na-pyrophosphate extractable and HCl-insoluble organic matter, OM_{ER} organic matter in the residue, ns not significant

*Spearman rank

Transect scale

We hypothesized that the $\delta^{13}\text{C}$, $\delta^{15}\text{N}$, and OC content pattern of OM fractions across the transects to be a result of land management or isotopic effects that occur with erosion, OM production, and turnover. We used the Rayleigh distillation model as a general test to infer if land management versus isotopic fractionation explained patterns in OM content and isotopic values.

Distinct differences in the rate of OM transformation exist between the different fractions, specifically between two groups: 1) the organic particle (OP) and Na-pyrophosphate extractable and HCl-insoluble organic matter (OM_{PYP}) fractions, versus 2) the Na-pyrophosphate extractable and HCl-soluble organic matter (OM_{PYS}) and organic matter in the extraction residue (OM_{ER}) fractions. The Rayleigh slopes of the OP fractions were significantly lower, indicating a slower turnover rate overall. The OP fractions are most likely representative of recent un-decomposed plant litter, the absence of a pattern in the ^{15}N Rayleigh model supports this assumption as land management effects and plant species selection contribute to the variability. The OM_{PYP} fractions, on the other hand, represent OM that is mineral-associated and that has been microbially processed (Kayler et al. 2011). The turnover rate, inferred from the slope of the Rayleigh model, is the slowest of the stabilized OM fractions,

and is thus potentially moving more slowly down the hillslope. Based on the steeper slopes of the Rayleigh model, we found that the OM_{ER} and OM_{PYS} fractions had the fastest landscape turnover time and could be related to transport due to the small size or a preference in the type of OM binding, a possibility described in depth below. Furthermore, the faster turnover of the OM_{PYS} fractions relative to the OM_{PYP} was consistent for both C and N. These findings suggest different processes are affecting the rates of transformations that are recorded in the isotopic composition patterns. Despite the differences in turnover rates, we did find similar $\delta^{13}\text{C}$ and $\delta^{15}\text{N}$ Rayleigh patterns (i.e., the slopes are all negative) for OM bound by mineral associations, fractions that contributed to the majority (> 65%) of OM_{bulk}: OM_{PYS}, OM_{PYP}, and the OM_{ER} fractions. We propose that there are at least two non-mutually exclusive explanations for the patterns we observed that can be generalized into biological and transport related isotope effects.

The linear statistical model (LME) identified LAI, a proxy of plant productivity, as a significant variable that explains the variation of $\delta^{13}\text{C}$ along the transect (Table 5). LAI was greater in positions closer to the kettle hole and corresponds to more negative values of OM $\delta^{13}\text{C}$, presumably sites near the kettle hole are more favorable to plant growth which can lead to

greater isotopic discrimination during photosynthesis and consequently OM depleted in ^{13}C (Brüggemann et al. 2011). We acknowledge that LAI is only a proxy for plant growth and subsequent C reaching sites of stabilization within soil, and we need to assume that productivity has been maintained over SOM development time scales (Gerke et al. 2016), but a plant response to the transect gradient would explain the trend toward more negative isotopic values from hilltop to edge. In this case, the system is open and OM is repeatedly introduced for stabilization, a process often referred to as dynamic replacement (Berhe et al. 2007, 2008; Harden et al. 1999).

The second explanation of the Rayleigh results, with an emphasis on the mineral associated fractions, is the transport of OM, soil particles, and aggregates during erosion. Based on their settling velocities, the smallest particles and aggregates are selectively transported furthest along the hillslope (Hu et al. 2016). This leads to an enrichment of clay and silt at depositional sites, in our case, the kettle hole sediments. Fine particles and aggregates especially $< 53\ \mu\text{m}$ are generally comprised of complexed, poorly crystalline and well-crystallized mineral phases as well as clay minerals (e.g., oxides, layer-silicates), which can interact with OM (Kaiser et al. 2007; Wagai et al. 2013; Doetterl et al. 2015). We therefore hypothesize that these fine particles and aggregates are associated with OM that is relatively depleted in ^{13}C and ^{15}N explaining the patterns of the mineral associated fractions OM_{PYS} , OM_{PYP} and OM_{ER} across the topographic positions. These results are consistent with the findings of Kaiser et al. (2001), who found that sorption led to a depletion in ^{13}C in the hydrophobic fraction that preferentially bound to mineral surfaces, providing a mechanism for our findings. In one of the most in-depth studies to date on particle size and corresponding isotopic values, Hu et al. (2016) found a depletion in ^{13}C and a higher OC content with decreasing particle size independent from topographic position. In our study, we discuss the possible mechanisms behind the association of OM with poorly crystalline and well-crystallized mineral phases in the aggregate scale discussion below (section “Aggregate scale”).

The non-mineral associated organic particle (OP) and water-extractable organic matter (WEOM) fractions exhibit origins from plant inputs, effects from land management, and transformations from microbial

decomposition. For example, the loosely bound organic particles (OP_{free}) can be regarded as fresh, poorly decomposed OM, and therefore reflects plant C isotopic composition. However, the overall $\delta^{15}\text{N}$ of OP_{free} does not conform to the Rayleigh distillation patterns (Fig. 6). Such inconsistencies may result from slurry fertilization, which is known to lead to an enrichment in ^{15}N of plants (Bateman et al. 2005; Senbayram et al. 2008). The downslope transport of slurry and nutrients (Lloyd et al. 2016) may subsequently have led to enrichment in ^{15}N at the footslopes and edges (Choi et al. 2003).

We observed a pattern of isotopic enrichment in the water extractable fractions that may result from decomposition of OM, supply of OM to soil, or slurry application. Enrichment in ^{13}C and ^{15}N of bulk soil OM is often attributed to the processing of soil OM by microbes (Dijkstra et al. 2008; Kayler et al. 2011; Brüggemann et al. 2011). The aggregate-bound water-extractable organic matter (WEOM_{A}) isotopic values were consistently elevated compared to the loosely attached water-extractable organic matter ($\text{WEOM}_{\text{free}}$) (Table 4) indicating that WEOM_{A} represents OM with a larger degree of microbial processing. Furthermore, the enrichment of ^{15}N of WEOM fractions and the enrichment of ^{13}C of WEOM_{A} from the hilltop to kettle hole edge (Figs. 5, 6) suggests products of microbial decomposition may accumulate with transport and leach toward the kettle, or the conditions for decomposition increase along the transect. Slurry application might also have contributed to the enrichment in ^{15}N of $\text{WEOM}_{\text{free}}$ and WEOM_{A} via inorganic N in these fractions (Table 4). Gregorich et al. (2003) suggested inorganic N derived from manure to have led to low C:N ratios in water extractable fractions, which is in agreement with our C:N ratios of the $\text{WEOM}_{\text{free}}$ and WEOM_{A} fractions. Alternatively, denitrification that may occur during periods of anoxia, which might have produced nitrate enriched in ^{15}N that was later incorporated in OM (Pennock et al. 1992; Sutherland et al. 1993; Dungait et al. 2013).

Based on the decreasing trend of isotopic values with OC content, we can confirm our first hypothesis, that at the transect scale OM patterns are largely driven by material transport and inputs from plant productivity and, to a lesser extent, land management. Microbial processing was an important factor in the OM isotopic patterns of WEOM fractions along the

transect; however, the role of microbes may also still be relevant at the aggregate scale.

Aggregate scale

The transect provided a strong gradient in clay, silt, and cation concentrations as well as different forms of Fe and Al that allowed us to infer OM stabilization dynamics in the soil. Our OC recovery rate of 84–96% (Fig. 4) was similar to other studies (Balesdent et al. 1998; Moni et al. 2012) and indicated that we lost a part of OC that we attribute to the vacuum filtration especially after the ultrasonication, which was of higher importance for the clay rich sediments. As such, we might have slightly underestimated the OC contents of the OM_{PYS}, OM_{PYP}, and OM_{ER} fractions. We observed > 65% of OC in putative stabilized fractions OM_{PYS}, OM_{PYP}, and OM_{ER} highlighting the

importance of organo-mineral interactions. The strong positive correlations between organically complexed Fe (Fe_{PYT}) and Al (Al_{PYT}) with OC in the Na-pyrophosphate extractable organic matter (OM_{PYS}, OM_{PYP}) fractions (Table 6) indicate the occurrence of Fe-OM and Al-OM associations (Fig. 7). Furthermore, correlations between the poorly crystalline Fe (Fe_{ox}) content with OM_{PYS} and OM_{PYP} suggests that poorly crystalline Fe oxides may also be involved in binding OM.

The distribution of polyvalent cations at topographic positions provides evidence for erosion of certain Fe phases. At the footslopes and edges we found the largest Fe_{PYT}, Fe_{ox}, Al_{PYT}, and OC contents (Fig. 3; Table 4), similar to Berhe et al. (2012) and Ellerbrock et al. (2016), indicating the downslope transport of poorly crystalline and organically complexed Fe and Al phases. In addition, moister

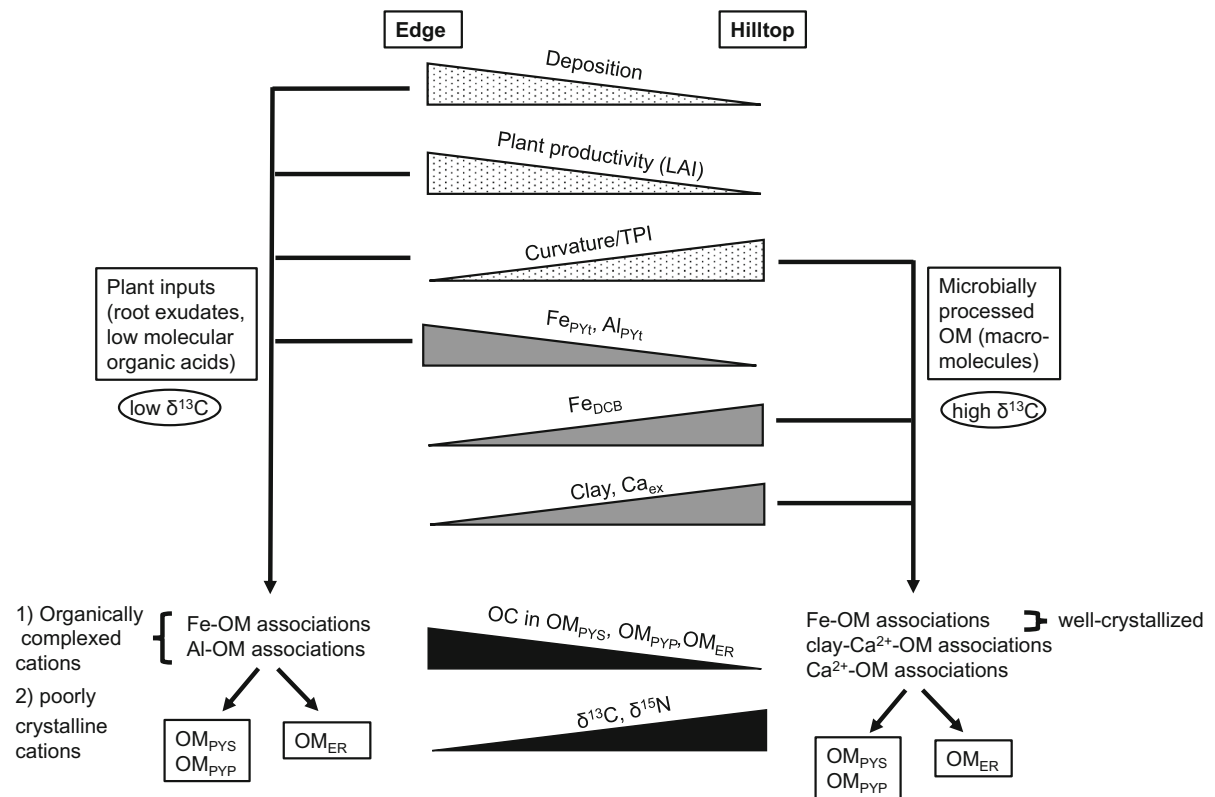


Fig. 7 Conceptual model illustrating the origin and parameters as well as pathways and processes that affect the fate of Na-pyrophosphate extractable and HCl-soluble organic matter (OM_{PYS}), Na-pyrophosphate extractable and HCl-insoluble organic matter (OM_{PYP}) and organic matter in the extraction residue (OM_{ER}) across a transect from erosional (right) to

depositional (left) areas. The elongated triangles illustrate an increase or decrease of a given process or parameter across the transect. OM was regarded as associated with minerals based on correlations of $\delta^{13}\text{C}$, $\delta^{15}\text{N}$ and OC contents with soil mineral characteristics (Table 6) and on the significant effects obtained from the linear mixed effects model (Table 5)

conditions in the vicinity of the kettle hole could lead to the transformation of well-crystallized Fe phases into poorly crystalline and organically complexed Fe phases in the depositional area (footslopes, edges) (Thompson et al. 2011). In contrast, we found greater concentrations of well-crystallized Fe phases (Fe_{DCB}) at hilltops and hillslopes due to more oxic conditions. This is indicated by the increase in the $\text{Fe}_{\text{ox}}:\text{Fe}_{\text{DCB}}$ and $\text{Fe}_{\text{PYt}}:\text{Fe}_{\text{DCB}}$ ratios toward the kettle hole (Fig. 3). Such patterns suggest that soil from eroding positions may have maximized the capacity to stabilize OM via organo-mineral complexes (Berhe et al. 2012).

We found negative correlations between Fe_{PYt} , Fe_{ox} and Al_{PYt} with $\delta^{13}\text{C}$ and $\delta^{15}\text{N}$ (Table 6) suggesting that poorly microbially processed OM is stabilized via Fe-OM and Al-OM associations. We contend that there is a preferential sorption of recent plant assimilates (e.g., root exudates) that are depleted in ^{13}C and ^{15}N (Kaiser et al. 2001). However, the permanence of mineral associated OM is uncertain, as hypotheses exist that suggest root-derived OM is protected from microbial decomposition (Farrar et al. 2003; Rasse et al. 2005) while other research shows oxalic acid derived from roots liberates mineral associated OM (Keiluweit et al. 2015). Both concepts can explain the patterns we observed in our data. Isotopically light material associates with mineral surfaces that may become protected from decomposition or lost, freeing up binding sites that are then reoccupied later.

On the other hand, the observed enrichment in ^{13}C of OM_{PYS} , OM_{PYP} and OM_{ER} with increased Fe_{DCB} contents suggests more microbially processed OM is stabilized with well-crystallized Fe phases (Fig. 7). Furthermore, the positive correlations between $\delta^{13}\text{C}$ of OM_{PYS} , OM_{PYP} and OM_{ER} with the contents of Ca_{ex} and clay (Table 6) indicates interactions of OM either directly with Ca^{2+} or via Ca^{2+} with clay-sized Al-silicates (Kayler et al. 2011). Since Fe_{DCB} , Ca_{ex} and clay contents are higher at hilltops and hillslopes, organo-mineral associations are particularly important at these erosional areas, corroborating the findings of Berhe et al. (2012). Interestingly, OC contents of OM_{PYS} and OM_{PYP} were negatively correlated with Fe_{DCB} , Ca_{ex} , and clay contents, which contradicts the findings of Kaiser et al. (2012) for Ca_{ex} . We attribute our findings to the transport of OM downslope and lower plant productivity at eroding positions. Overall, we confirm hypothesis (2), OM at our site was

stabilized by different mineral associations that are slope position dependent; moreover, we found that the OM bound in the different organo-mineral associations range from recent plant inputs to microbially processed material.

Sedimentary organic matter

The kettle hole is clearly collecting and accumulating OM. We hypothesized that the source of this OM in the sediment fractions was of different terrestrial origin. The depleted isotopic values of the mineral-associated OM sediment fractions largely conform to the Rayleigh model, but not in terms of the very high OC and TN concentrations of the kettle holes (Figs. 5, 6). The isotopic results are consistent with the framework of a large input of OM depleted in the heavy isotopes transported with small particles such as clay, and silt into the kettle hole, as discussed for the transect results (section “[Transect scale](#)” above). The higher OC contents of the mineral-associated OM fractions compared to SOM fractions is most likely due to the accumulation of transported material over time (Stallard 1998) and is confirmed by the high C stock in the sediment. Furthermore, molar C:N ratios of aquatic sedimentary OM fractions are in a similar range compared to C:N ratios from SOM fractions. This finding suggests the presence of pond-internal aquatic sources, such as phytoplankton or other periphytic algae, with molar C:N ratios typically ranging from 4 to 10 (Meyers 1994), unlikely. Therefore, our molar C:N ratios > 12 from organic particles (OP_{free} , OP_{A}) and Na-pyrophosphate extractable organic matter (OM_{PYS} , OM_{PYP}) (Table 4) are consistent with a terrestrial OM source.

However, macrophytes and inputs from land management are other potential OM sources that contribute to kettle hole sediments. Emergent macrophytes (*Carex acutiformis*, *Sparganium erectum*) are common in the littoral zone of the kettle hole. We regard emergent macrophytes as terrestrial in origin given their high lignin content and since atmospheric CO_2 is the C source. Furthermore, submerged, floating-leaved, and free-floating macrophytes are present in the kettle hole. We consider these macrophytes as aquatic in origin since dissolved inorganic carbon (DIC) is the C source. These macrophytes of aquatic and terrestrial origin represent a direct source of OM into the water column either

directly as particulate organic matter (POM) or as dissolved organic matter (DOM) after decay (Nitzsche et al. 2017) and can partly contribute to the high C stock in the sediment. Visible plant residues in organic particles (OP_{free} and OP_{A}) support this assumption, but we lack estimates of macrophyte productivity and isotopic signatures to properly estimate their contribution. Since we only separated the organic particles $> 63 \mu\text{m}$ after ultrasonication, we acknowledge macrophytes could contribute an unknown portion OC to the extraction residue OM_{ER} . In addition to macrophyte contributions, slurry application on the agricultural field may contribute to the $\delta^{15}\text{N}$ of OM fractions as suggested by Nitzsche et al. (2017) for a larger number of kettle holes located in agricultural fields. Based on these findings, we partly confirm hypothesis 3) that OM in sediment fractions is predominantly of terrestrial origin; however, with unknown contributions via aquatic OM and slurry sources.

Kleeberg et al. (2016) found that the sediment accretion rate increased after 1983 for the same kettle hole, due to the intensification of agriculture in the area (Bayerl 2006) leading to enhanced erosive inputs. OM was found to be associated with clay in marine sediments (Keil et al. 1994; Hedges and Oades 1997), and Lalonde et al. (2012), suggested a preferential stabilization of ^{13}C rich proteins and carbohydrates via reactive iron surfaces, which is a possibility for our sediments given the enriched $\delta^{13}\text{C}$ values of OM_{PYS} . Though our kettle hole replicate size ($n = 4$) is too small for robust correlation analyses, the large OC content of OM_{PYS} , OM_{PYP} and OM_{ER} fractions provide strong evidence for organo-mineral associations (Table 4).

Conclusions

We have shown that OM stabilization and accumulation along agricultural hillslopes is contingent upon relatively large-scale drivers, in our case, erosion and land management that enhances plant productivity. Organo-mineral associations with poorly crystalline mineral phases and organically complexed cations were clearly important where fine soil particles accumulated and we were able to demonstrate that the OM associated to these phases tended to be depleted in the heavy isotopes ^{13}C and ^{15}N . The

depleted isotopic signatures emphasize the role of recent plant assimilates in stabilized OM and the mechanism behind these patterns deserves further investigation. Similarly, the transport of fine soil particles and associated OM into kettle holes contributes to the large C storage potential of kettle holes in this hummocky, arable landscape. Overall, the combination of OM fractions and stable isotopes provided useful information concerning the source of OM and how OM is distributed within the kettle hole catchment. Accounting for the full range of particle sizes transported along the hillslope as well as quantifying the annual contributions of transported material to the kettle holes will help improve the understanding of OM dynamics in eroding agricultural landscapes.

Acknowledgements We thank Frau Remus, Dr. Sara Herrero Martín, and Ruben Yague for their help with the sample preparation and isotope analysis. We thank Kristina Holz and her team from the Central Laboratory at ZALF for measurements of the soil chemical characteristics as well as Michael Facklam from the Technische Universität Berlin for soil textural analysis. We also thank Renee Ende for support with OM fractionation. We kindly thank the LandScales team for their support and discussions. This research was funded through the Pact for Innovation and Research of the Gottfried Wilhelm Leibniz association (project LandScales—‘Connecting processes and structures driving landscape carbon dynamics over scales’). Finally, we thank two anonymous reviewers for their constructive comments, which have improved this manuscript.

References

- Amelung W, Zech W (1999) Minimisation of organic matter disruption during particle-size fractionation of grassland epipedons. *Geoderma* 92:73–85. doi:[10.1016/S0016-7061\(99\)00023-3](https://doi.org/10.1016/S0016-7061(99)00023-3)
- Balesdent J, Besnard E, Arrouays D, Chenu C (1998) The dynamics of carbon in particle-size fractions of soil in a forest-cultivation sequence. *Plant Soil* 201:49–57. doi:[10.1023/A:1004337314970](https://doi.org/10.1023/A:1004337314970)
- Bateman AS, Kelly SD, Jickells TD (2005) Nitrogen isotope relationships between crops and fertilizer: implications for using nitrogen isotope analysis as an indicator of agricultural regime. *J Agric Food Chem* 53:5760–5765. doi:[10.1021/jf050374h](https://doi.org/10.1021/jf050374h)
- Bayerl G (2006) Geschichte der Landnutzung in der Region Barnim-Uckermark. Materialien der Interdisziplinären Arbeitsgruppe Zukunftsorientierte Nutzung ländlicher Räume—Land Innovation Nr. 12., Berlin-Brandenburgische Akademie der Wissenschaften, Berlin
- Berhe AA, Harte J, Harden JW, Torn MS (2007) The significance of the erosion-induced terrestrial carbon sink. *BioScience* 57:337–346. doi:[10.1641/B570408](https://doi.org/10.1641/B570408)

- Berhe AA, Harden JW, Torn MS, Harte J (2008) Linking soil organic matter dynamics and erosion-induced terrestrial carbon sequestration at different landform positions. *J Geophys Res Biogeosci* 113:G04039. doi:[10.1029/2008JG000751](https://doi.org/10.1029/2008JG000751)
- Berhe AA, Harden JW, Torn MS et al (2012) Persistence of soil organic matter in eroding versus depositional landform positions. *J Geophys Res Biogeosci* 117:G02019. doi:[10.1029/2011JG001790](https://doi.org/10.1029/2011JG001790)
- Bremner JM, Lees H (1949) Studies on soil organic matter: Part II. The extraction of organic matter from soil by neutral reagents. *J Agric Sci* 39:274–279. doi:[10.1017/S0021859600004214](https://doi.org/10.1017/S0021859600004214)
- Bremner JM, Heintze SG, Mann PJG, Lees H (1946) Metallo-organic complexes in Soil. *Nature* 158:790–791. doi:[10.1038/158790b0](https://doi.org/10.1038/158790b0)
- Brüggemann N, Gessler A, Kayler Z et al (2011) Carbon allocation and carbon isotope fluxes in the plant-soil-atmosphere continuum: a review. *Biogeosciences* 8:3457–3489. doi:[10.5194/bg-8-3457-2011](https://doi.org/10.5194/bg-8-3457-2011)
- Choi W-J, Ro H-M, Hobbie EA (2003) Patterns of natural ^{15}N in soils and plants from chemically and organically fertilized uplands. *Soil Biol Biochem* 35:1493–1500. doi:[10.1016/S0038-0717\(03\)00246-3](https://doi.org/10.1016/S0038-0717(03)00246-3)
- Cohen AS (2003) Paleolimnology: the history and evolution of lake systems. Oxford University Press, New York
- Cole JJ, Prairie YT, Caraco NF et al (2007) Plumbing the global carbon cycle: integrating inland waters into the terrestrial carbon budget. *Ecosystems* 10:171–184. doi:[10.1007/s10021-006-9013-8](https://doi.org/10.1007/s10021-006-9013-8)
- Conrad O, Bechtel B, Bock M et al (2015) System for automated geoscientific analyses (SAGA) v. 2.1.4. *Geosci Model Dev* 8:1991–2007. doi:[10.5194/gmd-8-1991-2015](https://doi.org/10.5194/gmd-8-1991-2015)
- Deumlich D, Schmidt R, Sommer M (2010) A multiscale soil-landform relationship in the glacial-drift area based on digital terrain analysis and soil attributes. *J Plant Nutr Soil Sci* 173:843–851. doi:[10.1002/jpln.200900094](https://doi.org/10.1002/jpln.200900094)
- Dijkstra P, LaViolette CM, Coyle JS et al (2008) ^{15}N enrichment as an integrator of the effects of C and N on microbial metabolism and ecosystem function. *Ecol Lett* 11:389–397. doi:[10.1111/j.1461-0248.2008.01154.x](https://doi.org/10.1111/j.1461-0248.2008.01154.x)
- DIN 19684–6 (1997) Methods of soil investigations for agricultural engineering—chemical laboratory tests—Part 6: determination of iron soluble in oxalate solution. Beuth Verlag, Berlin
- DIN ISO 10390 (1997) Soil quality—determination of pH (ISO 10390:2005). Beuth Verlag, Berlin
- DIN ISO 10694 (1995) Soil quality—determination of organic and total carbon after dry combustion (elementary analysis). Beuth Verlag, Berlin
- DIN ISO 11260 (1994) Soil quality—determination of effective cation exchange capacity and base saturation level using barium chloride solution (ISO 11260:2011). Beuth Verlag, Berlin
- DIN ISO 11277 (2002) Soil quality—determination of particle size distribution in mineral soil material—method by sieving and sedimentation (ISO 11277:2009). Beuth Verlag, Berlin
- Doetterl S, Cornelis JT, Six J et al (2015) Soil redistribution and weathering controlling the fate of geochemical and physical carbon stabilization mechanisms in soils of an eroding landscape. *Biogeosciences* 12:1357–1371. doi:[10.5194/bg-12-1357-2015](https://doi.org/10.5194/bg-12-1357-2015)
- Doetterl S, Berhe AA, Nadeu E et al (2016) Erosion, deposition and soil carbon: A review of process-level controls, experimental tools and models to address C cycling in dynamic landscapes. *Earth-Sci Rev* 154:102–122. doi:[10.1016/j.earscirev.2015.12.005](https://doi.org/10.1016/j.earscirev.2015.12.005)
- Dungait JAJ, Ghee C, Rowan JS et al (2013) Microbial responses to the erosional redistribution of soil organic carbon in arable fields. *Soil Biol Biochem* 60:195–201. doi:[10.1016/j.soilbio.2013.01.027](https://doi.org/10.1016/j.soilbio.2013.01.027)
- Ellerbrock RH, Gerke HH, Deumlich D (2016) Soil organic matter composition along a slope in an erosion-affected arable landscape in North East Germany. *Soil Tillage Res* 156:209–218. doi:[10.1016/j.still.2015.08.014](https://doi.org/10.1016/j.still.2015.08.014)
- Farrar J, Hawes M, Jones D, Lindow S (2003) How roots control the flux of carbon to the rhizosphere. *Ecology* 84:827–837. doi:[10.1890/0012-9658\(2003\)084\[0827:HRCTFO\]2.0.CO;2](https://doi.org/10.1890/0012-9658(2003)084[0827:HRCTFO]2.0.CO;2)
- Fry B (2006) Stable isotope ecology. Springer, New York
- Gerke HH, Rieckh H, Sommer M (2016) Interactions between crop, water, and dissolved organic and inorganic carbon in a hummocky landscape with erosion-affected pedogenesis. *Soil Tillage Res* 156:230–244. doi:[10.1016/j.still.2015.09.003](https://doi.org/10.1016/j.still.2015.09.003)
- Gregorich EG, Beare MH, Stoklas U, St-Georges P (2003) Biodegradability of soluble organic matter in maize-cropped soils. *Geoderma* 113:237–252. doi:[10.1016/S0016-7061\(02\)00363-4](https://doi.org/10.1016/S0016-7061(02)00363-4)
- Harden JW, Sharpe JM, Parton WJ et al (1999) Dynamic replacement and loss of soil carbon on eroding cropland. *Global Biogeochem Cycles* 13:885–901. doi:[10.1029/1999GB900061](https://doi.org/10.1029/1999GB900061)
- Harris D, Horwath WR, van Kessel C (2001) Acid fumigation of soils to remove carbonates prior to total organic carbon or carbon-13 isotopic analysis. *Soil Sci Soc Am J* 65:1853–1856. doi:[10.2136/sssaj2001.1853](https://doi.org/10.2136/sssaj2001.1853)
- Hedges JI, Keil RG (1995) Sedimentary organic matter preservation: an assessment and speculative synthesis. *Mar Chem* 49:137–139. doi:[10.1016/0304-4203\(95\)00008-F](https://doi.org/10.1016/0304-4203(95)00008-F)
- Hedges JI, Oades JM (1997) Comparative organic geochemistries of soils and marine sediments. *Org Geochem* 27:319–361. doi:[10.1016/S0146-6380\(97\)00056-9](https://doi.org/10.1016/S0146-6380(97)00056-9)
- Hu Y, Berhe AA, Fogel ML et al (2016) Transport-distance specific SOC distribution: Does it skew erosion induced C fluxes? *Biogeochemistry* 128:339–351. doi:[10.1007/s10533-016-0211-y](https://doi.org/10.1007/s10533-016-0211-y)
- Kaiser K, Guggenberger G, Zech W (2001) Isotopic fractionation of dissolved organic carbon in shallow forest soils as affected by sorption. *Eur J Soil Sci* 52:585–597. doi:[10.1046/j.1365-2389.2001.00407.x](https://doi.org/10.1046/j.1365-2389.2001.00407.x)
- Kaiser K, Mikutta R, Guggenberger G (2007) Increased stability of organic matter sorbed to ferrihydrite and goethite on aging. *Soil Sci Soc Am J* 71:711–719. doi:[10.2136/sssaj2006.0189](https://doi.org/10.2136/sssaj2006.0189)
- Kaiser M, Ellerbrock RH, Sommer M (2009) Separation of coarse organic particles from bulk surface soil samples by electrostatic attraction. *Soil Sci Soc Am J* 73:2118–2130. doi:[10.2136/sssaj2009.0046](https://doi.org/10.2136/sssaj2009.0046)
- Kaiser M, Wirth S, Ellerbrock RH, Sommer M (2010) Microbial respiration activities related to sequentially separated, particulate and water-soluble organic matter fractions from

- arable and forest topsoils. *Soil Biol Biochem* 42:418–428. doi:[10.1016/j.soilbio.2009.11.018](https://doi.org/10.1016/j.soilbio.2009.11.018)
- Kaiser M, Ellerbrock RH, Wulf M et al (2012) The influence of mineral characteristics on organic matter content, composition, and stability of topsoils under long-term arable and forest land use. *J Geophys Res Biogeosci* 117:G02018. doi:[10.1029/2011JG001712](https://doi.org/10.1029/2011JG001712)
- Kaiser M, Zederer DP, Ellerbrock RH et al (2016) Effects of mineral characteristics on content, composition, and stability of organic matter fractions separated from seven forest topsoils of different pedogenesis. *Geoderma* 263:1–7. doi:[10.1016/j.geoderma.2015.08.029](https://doi.org/10.1016/j.geoderma.2015.08.029)
- Kaletka T, Rudat C (2006) Hydrogeomorphic types of glacially created kettle holes in North-East Germany. *Limnologica* 36:54–64. doi:[10.1016/j.limno.2005.11.001](https://doi.org/10.1016/j.limno.2005.11.001)
- Kayler ZE, Kaiser M, Gessler A et al (2011) Application of $\delta^{13}\text{C}$ and $\delta^{15}\text{N}$ isotopic signatures of organic matter fractions sequentially separated from adjacent arable and forest soils to identify carbon stabilization mechanisms. *Biogeosciences* 8:2895–2906. doi:[10.5194/bg-8-2895-2011](https://doi.org/10.5194/bg-8-2895-2011)
- Keil RG, Tsamakis E, Fuh CB et al (1994) Mineralogical and textural controls on the organic composition of coastal marine sediments: hydrodynamic separation using SPLITT-fractionation. *Geochim Cosmochim Acta* 58:879–893. doi:[10.1016/0016-7037\(94\)90512-6](https://doi.org/10.1016/0016-7037(94)90512-6)
- Keiluweit M, Bougoure JJ, Nico PS et al (2015) Mineral protection of soil carbon counteracted by root exudates. *Nat Clim Chang* 5:588–595. doi:[10.1038/nclimate2580](https://doi.org/10.1038/nclimate2580)
- Kirkels FMSA, Cammeraat LH, Kuhn NJ (2014) The fate of soil organic carbon upon erosion, transport and deposition in agricultural landscapes—a review of different concepts. *Geomorphology* 226:94–105. doi:[10.1016/j.geomorph.2014.07.023](https://doi.org/10.1016/j.geomorph.2014.07.023)
- Kleber M, Eusterhues K, Keiluweit M et al (2015) Mineral-organic associations: formation, properties, and relevance in soil environments. *Adv Agron* 130:1–140. doi:[10.1016/b.s.agron.2014.10.005](https://doi.org/10.1016/b.s.agron.2014.10.005)
- Kleeberg A, Neyen M, Schkade U-K et al (2016) Sediment cores from kettle holes in NE Germany reveal recent impacts of agriculture. *Environ Sci Pollut Res* 23:7409–7424. doi:[10.1007/s11356-015-5989-y](https://doi.org/10.1007/s11356-015-5989-y)
- Kuznetsova A, Brockhoff PB, Christensen RHB (2016) lmerTest: tests in linear mixed effects models
- Lalonde K, Mucci A, Ouellet A, Gélinas Y (2012) Preservation of organic matter in sediments promoted by iron. *Nature* 483:198–200. doi:[10.1038/nature10855](https://doi.org/10.1038/nature10855)
- Liu F, Zhang G-L, Sun Y-J et al (2013) Mapping the three-dimensional distribution of soil organic matter across a subtropical hilly landscape. *Soil Sci Soc Am J* 77:1241–1253. doi:[10.2136/sssaj2012.0317](https://doi.org/10.2136/sssaj2012.0317)
- Lloyd CEM, Michaelides K, Chadwick DR et al (2016) Runoff- and erosion-driven transport of cattle slurry: linking molecular tracers to hydrological processes. *Biogeosciences* 13:551–566. doi:[10.5194/bg-13-551-2016](https://doi.org/10.5194/bg-13-551-2016)
- Masiello CA, Chadwick OA, Southon J et al (2004) Weathering controls on mechanisms of carbon storage in grassland soils. *Global Biogeochem Cycles* 18:GB4023. doi:[10.1029/2004GB002219](https://doi.org/10.1029/2004GB002219)
- Mayer LM (1994) Surface area control of organic carbon accumulation in continental shelf sediments. *Geochim Cosmochim Acta* 58:1271–1284. doi:[10.1016/0016-7037\(94\)90381-6](https://doi.org/10.1016/0016-7037(94)90381-6)
- Meyers PA (1994) Preservation of elemental and isotopic source identification of sedimentary organic matter. *Chem Geol* 114:289–302. doi:[10.1016/0009-2541\(94\)90059-0](https://doi.org/10.1016/0009-2541(94)90059-0)
- Mikutta R, Kleber M, Torn MS, Jahn R (2006) Stabilization of soil organic matter: association with minerals or chemical recalcitrance? *Biogeochemistry* 77:25–56. doi:[10.1007/s10533-005-0712-6](https://doi.org/10.1007/s10533-005-0712-6)
- Mikutta R, Mikutta C, Kalbitz K et al (2007) Biodegradation of forest floor organic matter bound to minerals via different binding mechanisms. *Geochim Cosmochim Acta* 71:2569–2590. doi:[10.1016/j.gca.2007.03.002](https://doi.org/10.1016/j.gca.2007.03.002)
- Moni C, Derrien D, Hatton P-J et al (2012) Density fractions versus size separates: does physical fractionation isolate functional soil compartments? *Biogeosciences* 9:5181–5197. doi:[10.5194/bg-9-5181-2012](https://doi.org/10.5194/bg-9-5181-2012)
- Mouvenchery YK, Kučerík J, Diehl D, Schaumann GE (2012) Cation-mediated cross-linking in natural organic matter: a review. *Rev Environ Sci Biotechnol* 11:41–54. doi:[10.1007/s11157-011-9258-3](https://doi.org/10.1007/s11157-011-9258-3)
- Nitzsche KN, Verch G, Premke K et al (2016) Visualizing land-use and management complexity within biogeochemical cycles of an agricultural landscape. *Ecosphere* 7:e01282. doi:[10.1002/ecs2.1282](https://doi.org/10.1002/ecs2.1282)
- Nitzsche KN, Kaletka T, Premke K et al (2017) Land-use and hydroperiod affect kettle hole sediment carbon and nitrogen biogeochemistry. *Sci Total Environ* 574:46–56. doi:[10.1016/j.scitotenv.2016.09.003](https://doi.org/10.1016/j.scitotenv.2016.09.003)
- Pennock DJ, van Kessel C, Farrell RE, Sutherland RA (1992) Landscape-scale variations in denitrification. *Soil Sci Soc Am J* 56:770–776. doi:[10.2136/sssaj1992.03615995005600030016x](https://doi.org/10.2136/sssaj1992.03615995005600030016x)
- Premke K, Attermeyer K, Augustin J et al (2016) The importance of landscape complexity for carbon fluxes on the landscape level: small-scale heterogeneity matters. *WIREs Water*. doi:[10.1002/wat2.1147](https://doi.org/10.1002/wat2.1147)
- Rasse DP, Rumpel C, Dignac MF (2005) Is soil carbon mostly root carbon? Mechanisms for a specific stabilisation. *Plant Soil* 269:341–356. doi:[10.1007/s11104-004-0907-y](https://doi.org/10.1007/s11104-004-0907-y)
- Schlichting E, Blume H-P, Stahr K (1995) *Bodenkundliches Praktikum*. Blackwell, Berlin
- Schrumpf M, Kaiser K (2015) Large differences in estimates of soil organic carbon turnover in density fractions by using single and repeated radiocarbon inventories. *Geoderma* 239–240:168–178. doi:[10.1016/j.geoderma.2014.09.025](https://doi.org/10.1016/j.geoderma.2014.09.025)
- Senbayram M, Dixon L, Goulding KWT, Bol R (2008) Long-term influence of manure and mineral nitrogen applications on plant and soil ^{15}N and ^{13}C values from the Broadbalk Wheat Experiment. *Rapid Commun Mass Spectrom* 22:1735–1740. doi:[10.1002/rcm.3548](https://doi.org/10.1002/rcm.3548)
- Sollins P, Kramer MG, Swanston C et al (2009) Sequential density fractionation across soils of contrasting mineralogy: evidence for both microbial- and mineral-controlled soil organic matter stabilization. *Biogeochemistry* 96:209–231. doi:[10.1007/s10533-009-9359-z](https://doi.org/10.1007/s10533-009-9359-z)
- Stallard RF (1998) Terrestrial sedimentation and the carbon cycle: Coupling weathering and erosion to carbon burial. *Global Biogeochem Cycles* 12:231–257. doi:[10.1029/98GB00741](https://doi.org/10.1029/98GB00741)

- Sutherland RA, van Kessel C, Farrell RE, Pennock DJ (1993) Landscape-scale variations in plant and soil nitrogen-15 natural abundance. *Soil Sci Soc Am J* 57:169–178. doi:[10.2136/sssaj1993.03615995005700010031x](https://doi.org/10.2136/sssaj1993.03615995005700010031x)
- Thompson A, Rancourt DG, Chadwick OA, Chorover J (2011) Iron solid-phase differentiation along a redox gradient in basaltic soils. *Geochim Cosmochim Acta* 75:119–133. doi:[10.1016/j.gca.2010.10.005](https://doi.org/10.1016/j.gca.2010.10.005)
- von Lützow MV, Kögel-Knabner I, Ekschmitt K et al (2006) Stabilization of organic matter in temperate soils: mechanisms and their relevance under different soil conditions—a review. *Eur J Soil Sci* 57:426–445. doi:[10.1111/j.1365-2389.2006.00809.x](https://doi.org/10.1111/j.1365-2389.2006.00809.x)
- Wagai R, Mayer LM, Kitayama K, Shirato Y (2013) Association of organic matter with iron and aluminum across a range of soils determined via selective dissolution techniques coupled with dissolved nitrogen analysis. *Biogeochemistry* 112:95–109. doi:[10.1007/s10533-011-9652-5](https://doi.org/10.1007/s10533-011-9652-5)
- Wattel-Koekkoek EJW, Buurman P, Van Der Plicht J et al (2003) Mean residence time of soil organic matter associated with kaolinite and smectite. *Eur J Soil Sci* 54:269–278. doi:[10.1046/j.1365-2389.2003.00512.x](https://doi.org/10.1046/j.1365-2389.2003.00512.x)

Biogeochemistry is a copyright of Springer, 2017. All Rights Reserved.